

Alloy Nanocatalysts for the Electrochemical Oxygen Reduction (ORR) and the Direct Electrochemical Carbon Dioxide Reduction Reaction (CO₂RR)

Cheonghee Kim, Fabio Dionigi, Vera Beermann, Xingli Wang, Tim Möller, and Peter Strasser*

In the face of the global energy challenge and progressing global climate change, renewable energy systems and components, such as fuel cells and electrolyzers, which close the energetic oxygen and carbon cycles, have become a technology development priority. The electrochemical oxygen reduction reaction (ORR) and the direct electrochemical carbon dioxide reduction reaction (CO₂RR) are important electrocatalytic processes that proceed at gas diffusion electrodes of hydrogen fuel cells and CO₂ electrolyzers, respectively. However, their low catalytic activity (voltage efficiency), limited long-term stability, and moderate product selectivity (related to their Faradaic efficiency) have remained challenges. To address these, suitable catalysts are required. This review addresses the current state of research on Pt-based and Cu-based nanoalloy electrocatalysts for ORR and CO₂RR, respectively, and critically compares and contrasts key performance parameters such as activity, selectivity, and durability. In particular, Pt nanoparticles alloyed with transition metals, post-transition metals and lanthanides, are discussed, as well as the material characterization and their performance for the ORR. Then, bimetallic Cu nanoalloy catalysts are reviewed and organized according to their main reaction product generated by the second metal. This review concludes with a perspective on nanoalloy catalysts for the ORR and the CO₂RR, and proposes future research directions.

conversion of electricity and CO₂ into chemicals and fuels has therefore attracted heightened attention as it may contribute to a closed technological carbon cycle in the future.^[2] On the other hand, chemical fuels, such as hydrogen, can be reconverted to electricity via electrochemical reaction processes in fuel cells. The overall efficiency of fuel cells is severely hindered by sluggish kinetics of oxygen reduction reaction (ORR) at the cathode; in addition, their wider use has been impeded due to the high cost and loadings of platinum-based electrocatalysts. Electrochemical CO₂ reduction reaction (CO₂RR) is also energetically and atomically inefficient due to large kinetic overpotentials, and difficulties in controlling the chemical product selectivity, in particular the competition with the hydrogen evolution reaction in aqueous environments. This calls for improved catalysts with high efficiency, selectivity, and durability for both the ORR and CO₂RR. Among the many strategies currently considered such as support change, shape, and size control,^[3] alloy catalysts have proven effective to lower the


1. Introduction

In modern human society, energy generation and consumption has been largely relying on burning fossil fuels.^[1] Due to the limited reserves of fossil fuels and due to the long-term climatic consequences of the ever-increasing atmospheric concentration of the combustion byproduct CO₂, alternative, environmentally friendly renewable energy systems and energy system components are needed that will ensure a sustainable, since closed, technological carbon cycle. The electrochemical

kinetic overpotential and control the selectivity thanks to modified chemical binding of reactive intermediates on the catalyst surface due to changes in the electronic structure, geometric strain, and chemical bifunctionality.

The present progress report details progress and achievements in nanoalloy catalysts for two important catalytic multi-electron transfer reactions, the ORR and the CO₂RR (Figure 1). The ORR has two competing pathways toward H₂O₂ or H₂O, which are two-electron and four-electron transfer reactions, respectively. Pt emerged as one of the most active catalysts for the four-electron pathway, and one of the few elements that, at the same time, can reasonably withstand the harsh acidic and oxidizing conditions of the ORR environments in proton exchange membrane (PEM) fuel cells. On the other hand, the CO₂RR has a diverse set of chemical reaction pathways, depending on the electrode metal employed; for example, a two-electron transfer reduction produces CO or HCOO⁻, an eight-electron transfer reduction produces CH₄, a sixteen-electron transfer reduction produces C₂H₄, and even more electron transfer reductions are possible. Of all metals, Cu has been identified as unique in that it is able to produce a number of “beyond CO” product such

Dr. C. Kim, Dr. F. Dionigi, V. Beermann, X. Wang, T. Möller, Prof. P. Strasser
Department of Chemistry
Chemical Engineering Division
Technical University Berlin
10623 Berlin, Germany
E-mail: pstrasser@tu-berlin.de

 The ORCID identification number(s) for the author(s) of this article can be found under <https://doi.org/10.1002/adma.201805617>.

DOI: 10.1002/adma.201805617

as hydrocarbons or organic oxygenates such as aldehydes or alcohols. Here, we focus on Pt-based and Cu-based alloy catalysts for ORR and CO₂RR, respectively. First, we introduce Pt–M alloy nanoparticles with transition metal, post-transition metal and lanthanides, and alkaline earth (AE) metal, and discuss the materials in their characterization and performance in ORR. Then, Cu–M alloy with second metals, which are well known as CO₂RR catalysts, are also reviewed afterward. Finally, we summarize future electrochemical catalyst designs and propose the problems to be addressed.

2. Pt-Based Nanoalloys for the Electrochemical Oxygen Reduction Reaction

In this section, we address Pt-based alloy nanoparticle catalysts, where platinum is alloyed with transition metals (i.e., Ni, Co, Fe, Cu, Sc, Y, Zr, Hf, Pd, ...), post-transition metals (i.e., Pb), lanthanides (La, Ce, Pr, Sm, Gd, Tb, Dy, and Tm), and alkaline earth metals (i.e., Ca, Sr). We also include discussions on intermetallics (or ordered alloys), shaped alloy particles and core–shell structures, nanoframes, and other nanostructured particles, which form by dealloying of parent Pt alloy nanoparticles.

Alloying Pt with a second metal is a successful strategy to enhance the catalytic real-surface area-based activity (also referred to as specific or intrinsic ORR activity) as well as the Pt-mass normalized ORR activity (here denoted as mass activity, MA) for the purpose of decreasing the geometric electrode Pt loading and hence the total Pt mass in fuel cell stacks and ultimately vehicles. The microscopic mechanistic origin of Pt alloy effect was linked to electronic ligand effects, structural lattice strain effects, as well as ensemble effects.^[4,5] In the development of these catalysts, the rotating disk electrode (RDE) technique plays a central role as an initial screening method to characterize and downselect the best performing catalysts that will be eventually integrated in the cathode of a single fuel cell. **Figure 2** compares and contrasts reported Pt mass–based activity data as well as their electrochemical surface areas of recent Pt alloy ORR catalyst discussed in the following. First, we note that comparing RDE data requires much caution due to different protocols and parameters employed and the extreme sensitivity of this technique to minute changes of any of these parameters.^[6,7] Nonetheless, the first-of-its-kind comparison shown in Figure 2 provides a sense of the range of activity enhancement over pure Pt obtained by alloy nanoparticle catalysts. We conclude from Figure 2 that most of the recent works on Pt-based alloy nanoparticles report on catalysts with electrochemical surface area (ECSA) between 20 and 80 m² g_{Pt}⁻¹ and an initial mass activity evaluated at 0.9 V_{RHE} below 3 A mg_{Pt}⁻¹ (with few exceptions reaching much higher values, often however without any published independent reproduction). This MA is extraordinarily high, if we consider that state-of-the-art Pt/C nanoparticles typically show 1 order of magnitude lower MA values (i.e., ≈0.2–0.3 A mg_{Pt}⁻¹),^[6] while the ECSA of the alloy nanoparticles is in general lower or approaching the one of Pt/C (i.e., 60–70 m² g_{Pt}⁻¹).^[6] Stability is a major issue of many alloy nanoparticle catalysts and is discussed for the single cases. In the following, these works are reviewed and the future perspective is given.



Cheonghee Kim received her Ph.D. from the Department of Chemical and Biomolecular Engineering in 2013 at Yonsei University, Republic of Korea. Then, she worked at Korea Institute of Science and Technology (KIST) and Korea Advanced Institute of Science and Technology (KAIST) as a postdoctoral fellow until August 2016. Since then, she joined “The Electrochemical Energy, Catalysis, and Materials Science Group” in the Department of Chemical Engineering at Technische Universität Berlin, Germany. Her research is focused on Cu-based alloy catalysts for electrochemical CO₂ reduction reaction and design of novel catalysts for practical applications.



Vera Beermann received her M.Sc. in Chemistry at Technische Universität Berlin (TUB) in 2015, and then started her Ph.D. in “The Electrochemical Energy, Catalysis, and Materials Science Group” under Prof. Strasser at TUB. As a visiting Ph.D. student, she has collaborated with Prof. Muller (Cornell University, USA). She is currently pursuing her Ph.D. at TUB, focusing on the synthesis and characterization of size- and shape-controlled nanostructured materials for electrocatalytic applications.



Peter Strasser is the chaired professor of Electrochemistry and Electrocatalysis in the Chemical Engineering Division of the Department of Chemistry at the Technical University Berlin. Prior to his appointment, he was Assistant Professor at the Department of Chemical and Biomolecular Engineering at the University of Houston. Before moving to Houston, Prof. Strasser served as Senior Member of staff at Symyx Technologies, Inc., Santa Clara, USA. In 1999, Prof. Strasser received his Ph.D. in Physical Chemistry and Electrochemistry from the Fritz-Haber Institute of the Max-Planck-Society, Berlin, Germany, under the direction of Gerhard Ertl.

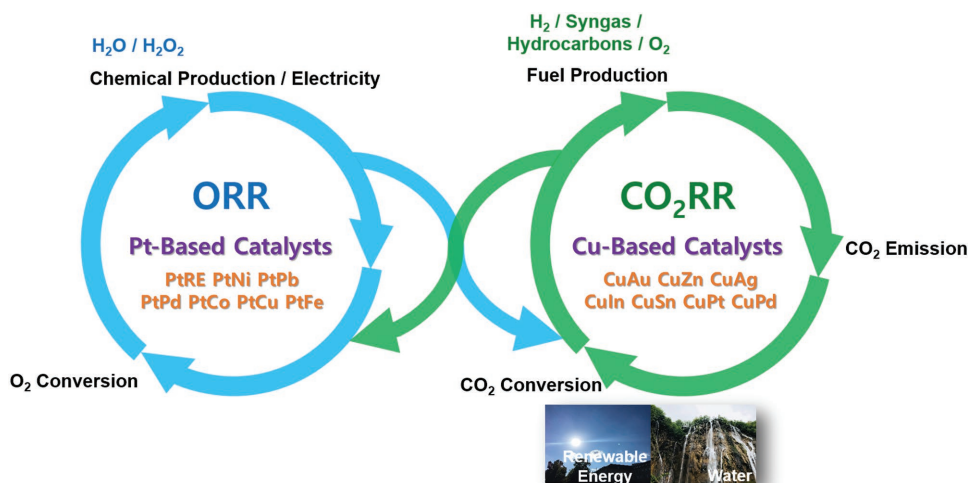


Figure 1. The oxygen reduction reaction (ORR) and the carbon dioxide reduction reactions (CO₂RR) exhibit close conceptual links as coupled multi-electron reduction processes for electrolytic and galvanic cells catalyzed by Pt-based catalyst (ORR) and Cu-based catalysts (CO₂RR), respectively.

2.1. Pt–Ni Alloys

Pt–Ni alloys constitute some of the most active catalyst candidates for the ORR. An enormously wide range of particle sizes, compositions, shapes, postsynthesis treatments, and electrochemical conditioning protocols have been investigated in recent years. Among those, spherical (note that in a stricter sense, spherical particles are still faceted particle, yet with a high degree of high-index facets) Pt–Ni alloyed/dealloyed, core–shell, and porous/hollow nanoparticles have been reported and used for ORR tests since the early 1990s. Nanoparticles in different sizes and compositions

were reported and studied in terms of their activity and stability, postsynthesis treatments, and electrochemical conditioning.^[8]

The surface of Pt₃Ni particles can be tuned from a very Pt-rich, balanced Pt–Ni alloy surface to a quite Ni-rich surface using thermal reduction at different temperatures for different times as reported by Zhang et al.^[9] The Pt-skin surface catalyst exhibits a 3.4× greater MA than pure Pt, which they attribute to the enhanced catalyst surface structure and the influence of their porous graphitic carbon support. Gan et al. developed a robust and simple synthesis approach that allows for the synthesis of sub-10 nm low Pt-content particles in different sizes and revealed a Volcano-shaped dependence of ORR activity and stability as a function of particles size.^[10] Recently, boron-doped Pt₃Ni alloys have been reported to enhance the electrochemical ORR activity in comparison to their undoped counterparts which the authors attribute to the slightly intensified adsorption strength of O-containing species.^[11] A large improvement of electrocatalytic durability was gained by Pt-alloy core–shell nanostructures with gold nanoparticles as core and Pt–Ni alloys as shells.^[12] Porous hollow nanoparticles were investigated with varying Ni content, lattice parameters, and specific surface areas, providing evidence for the positive influence of structural defects such as grain boundaries on the ORR kinetics.^[13] Up to date, spherical Pt–Ni alloy nanoparticles are still the most promising candidates for practical applications in fuel cell cathodes.^[14] This is because it was possible to reproduce their ideal RDE MA in a realistic layered electrode of a catalyst-coated membrane interfacing with a microporous layer, something that has not been possible with other shape controlled catalysts.^[15] Sets of catalyst particles have been investigated in order to transfer knowledge from RDE tests to the real MEA device. Small particle sizes and less-oxidative acid treatments in combination with annealing reduce Ni leaching and nanoporosity formation during MEA operation, resulting in a good and stable catalyst performance of dealloyed PtNi₃ catalysts.^[15]

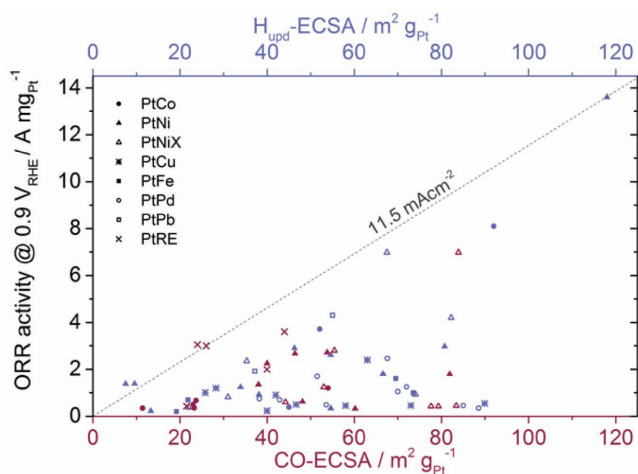


Figure 2. Recent achievements in oxygen reduction reaction mass activity for Pt-based alloys. Data points represent results obtained by rotating disk electrode and extracted from the recent works that are discussed in this perspective. The data were divided per alloy element and plotted as a function of the electrochemical surface area, either measured by hydrogen under potential deposition (H_{upd} -ECSA, blue) or by CO stripping (CO-ECSA, red). The dashed line corresponds to the specific activity of 11.5 mA cm⁻². For Pt–rare earth alloys the abbreviation PtRE is used.

Since Stamenkovic et al. reported about their findings on Pt₃Ni single crystals and their remarkable ORR performance in 2007,^[16] a lot of effort was attempted in order to develop tunable and robust synthesis protocols for octahedrally shaped Pt–Ni catalysts enclosed entirely by {111} facets.^[17,18] This shows that single crystal studies continue to remain of great importance to learn about detailed surface characteristics of alloy facets and to use these insights for the design innovative nanoscale catalyst materials.^[19]

The growth and degradation of PtNi-alloy nanoparticles have been compared and contrasted for octahedral particles produced by a solvothermal^[18] and a wet-chemical synthesis. **Figure 3a** shows the structural and composition evolution model for the wet-chemical synthesis approach.^[20] Both growth mechanisms

start from initial cuboctahedral Pt–Ni alloy seeds. Under solvothermal conditions, the {100} directions grow fastest producing transient hexapod-shaped nanoparticles with very Pt-rich arms, before a preferred Ni deposition sets in and fills the octahedra in all eight {111} crystallographic directions, until a self-terminated complete, yet a compositionally anisotropic octahedron is obtained.^[21]

Several works report on postsynthesis surface conditioning of Pt–Ni octahedra which includes besides strong acid or base treatment^[22] annealing as a powerful tool to induce octahedral facet healing^[23] and surface segregation^[24] to further improve the catalytic activity and electrochemical stability.^[25]

Pt–Ni octahedra suffer from rapid performance losses during electrochemical operation limiting their application

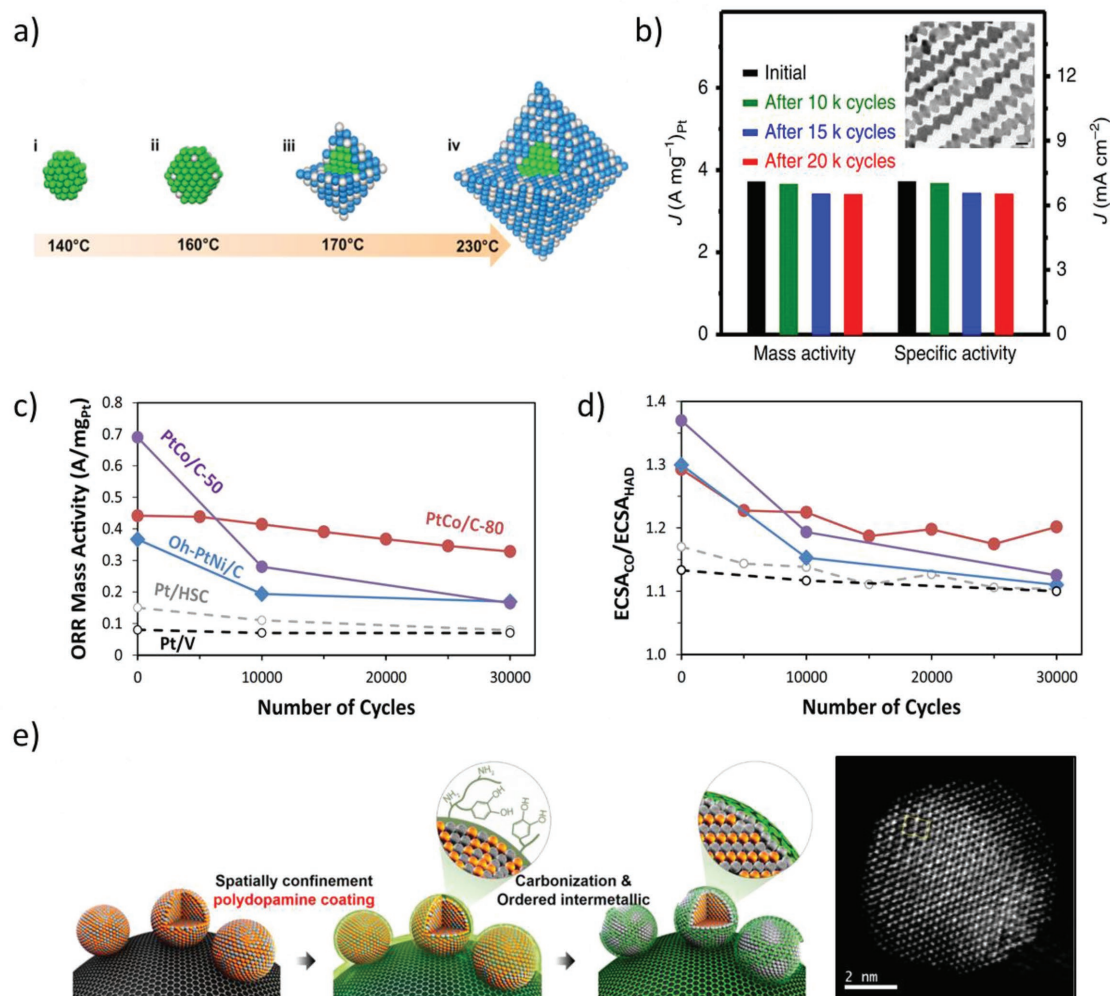


Figure 3. Pt-late 3d transition metal alloys: PtNi, PtCo, and PtFe. a) Growth of Pt–Ni octahedral nanoparticles prepared via a wet-chemical synthesis approach. Model shows the structural and composition evolution: i) spherical pure Pt seeds, to ii) truncated octahedron with small amounts of Ni, to iii) small octahedral particles with a Pt–Ni shell, to iv) the Pt–Ni octahedral in its final size and composition. Reproduced with permission.^[20] Copyright 2017, American Chemical Society. b) MA and specific activity of highly active Pt₃Co/ nanowires in their initial state, after 10 000, 15 000, and 20 000 potential cycles between 0.6 and 1.1 V_{RHE} with 100 m s⁻¹. Reproduced with permission.^[47] Copyright 2016, Springer Nature. c) Pt-based mass activity of different ORR catalysts measured in MEA as a function of cycle number. d) ECSA_{CO}/ECSA_{HAD} ratio as function of cycle number. Cycling was performed with 500 mV s⁻¹, 100% RH in H₂/N₂ cell. c,d) Reproduced with permission.^[49] Copyright 2016, ECS. e) Carbon-supported and N-doped carbon-coated ordered fct–PtFe nanoparticles: systematic synthesis diagram and HAADF-STEM image of a resulting particle. In a first step disordered fcc–PtFe particles are synthesized and supported on carbon. The fcc–PtFe/C was then coated with polydopamine and thermally annealed at 700 °C, forming the ordered fct–PtFe with the N-doped carbon shell. Reproduced with permission.^[73] Copyright 2015, American Chemical Society.

in real MEA devices.^[14] A crucial step to improve the stability of octahedral Pt–Ni alloy catalysts is to maintain the integrity and morphology of the active Pt–Ni {111} facets by protecting the less noble compound Ni from dissolution during electrochemical cycling in corrosive environments. Xia and co-workers reported improved stabilities and good activities for octahedral Pt–Ni@Pt_{1.5L} particles. After 10 000 cycles of electrochemical stress protocol, their Pt–Ni@Pt_{1.5L} lost only 25% of Ni, whereas their Pt–Ni references lost 75% of Ni.^[26] The group of Huang presented a systematic study on octahedral Pt–Ni particles doped with a set of transition metals and found a great enhancement in ORR activity (6.98 A mg_{Pt}⁻¹) and durability in terms of shape and ORR performance after 8000 potential cycles (6.60 A mg_{Pt}⁻¹) for Mo–PtNi.^[27] Doping with several other elements such as rhodium,^[28] halides^[29] or gallium^[30] has been described to be efficient to improve the durability. Besides surface doping with a third element, trimetallic systems were discussed. For example, Pt₂CuNi octahedral particles show a promising ORR activity (2.35 A mg_{Pt}⁻¹) and a remarkable durability after 10 000 cycles (1.60 A mg_{Pt}⁻¹).^[31]

Several other shapes were described to be excellent ORR catalysts as well. Duan and co-workers reported on ultrafine jagged platinum nanowires with a previously unreported, yet to the authors knowledge never publicly reproduced MA of 13.6 A mg_{Pt}⁻¹. Using reactive molecular dynamics simulations they could assign this enormous improvement to undercoordinated rhombus-rich surface configurations.^[32] Another family of shaped nanoparticles is *nanoframes* and *nanocages* that were studied extensively in terms of their growth mechanism, ORR activity and durability, and degradation mechanisms.^[33]

2.2. Pt–Co Alloys

Pt–Co alloys were extensively studied in terms of synthesis parameters, particles sizes and shapes, compositions, post-synthesis annealing treatments, and ORR activities in RDE and MEA setups.^[34–37] In contrast to Pt–Ni alloys, Pt–Co alloys can easily be converted into ordered alloys (intermetallics) by annealing at temperatures of 700 °C or higher. Pt₃Co core–shell particles were discussed by several groups as very active and stable ORR catalysts.^[35,38,39] The degradation mechanism of Pt₃Co/C nanocatalysts in MEAs after and during 10 000 cycles operation conditions was studied by Rasouli et al.^[40] Just recently, Wang et al. reported on ordered Pt₃Co intermetallic nanoparticles derived from metal-organic frameworks. They obtained highly ordered Pt₃Co particles after annealing at 900 °C in vacuum. Their particles showed significantly enhanced durability in RDE and MEA testing, strong resistance against metal dissolution, and good chemical stabilization on the carbon support.^[41] Hollow Pt₃Co/C particles were reported to exhibit a good ORR activity of 0.68 A mg_{Pt}⁻¹ and a remarkable durability after 5000 potential cycles.^[42]

Single crystal studies revealed a strong dependence of the Co content on the ORR activity in Pt-skin/Pt_{100-x}Co_x(111) electrodes. A remarkable 25× improvement in the catalytic ORR activity in comparison to the reference Pt(111) was observed at an atomic Co content of $x = 25\%$.^[43] In another study, the

authors compared different low index surface orientations and found the best ORR activity for Pt–Co (111) facets, but also the strongest dependence of Co contents.^[44]

Motivated by the results from Pt–Co single crystal studies, shape-selected Pt–Co nanoparticles were investigated. Chen et al. reported on excavated octahedral Pt–Co alloy nanocrystals, which besides being excellent ORR catalyst also show superior activities for the HER and MOR.^[45] Becknell et al. reported on the synthesis of polyhedral PtCo₃ nanoparticles and their evolution to Pt₃Co frames.^[36] High-index Pt–Co alloy surfaces were obtained by producing concave octahedron and cubes, correlating them with enhanced ORR activities.^[46] Pt₃Co nanowires attracted attention because of the highest ORR activity (3.71 A mg_{Pt}⁻¹) achieved for Pt–Co-based systems at that time and their outstanding durability after 20 000 potential cycles (3.41 A mg_{Pt}⁻¹). Figure 3b shows the changes in mass and specific activity of the particles in the initial state and after several cycles degradation protocol and a representative TEM image in the inset. Density functional theory (DFT) calculations suggest that the high ORR activities origin from the hollow side of the high-index facets.^[47] Just recently, Kongkanand and co-workers reported a breakthrough strategy to boost fuel cell performances by an optimal combination of ORR catalyst and support material. Pt–Co alloy catalysts supported on porous carbons with a preferred pore openings of 4–7 nm show optimized performance per gram Pt can be achieved.^[48] They also presented a comparative study on electrochemically active surface area measurements of aged Pt-based catalysts in a PEM fuel cell. They compared the ECSA values obtained by CO stripping and hydrogen adsorption/desorption, studied temperature effects on the resulting ECSA values, and Pt mass–based performances of different Pt-based materials, namely, Pt on Vulcan (Pt/V) and high surface area carbon (Pt/HSC), Pt–Co leached in nitric acid at different temperatures (PtCo/C-50, PtCo/C-80), and octahedral PtNi/C (Oh-PtNi). Figure 3c shows the ORR kinetic Pt-based mass activities of the different materials as a function of cycle number. PtCo/C-50 shows a good and stable performance over the whole number of cycles, while the other materials either show low initial activity or rapid performance losses. They also show that the ratio between ECSA_{CO} and ECSA_{Hupd} is not directly indicating the ORR activity (see Figure 3d).^[49]

For Pt–Co-based alloys, several trimetallic systems are described. Pd@Pt₃Co/C was tested in MEA devices and outperforms the tested reference materials Pt/C and Pd@Pt/C in activity and stability.^[50] Pt–Au–Co and Pt–Ir–Co alloys have been studied by Mitlin and co-workers. They kept the Pt–Co atomic ratio constant and systematically studied the ORR performance as a function of the Au and Ir amount and found an improved ORR activity for Pt_{72.5}Au_{2.5}Co₂₅ and dramatically improved corrosion stability with increasing amounts of Au and Ir.^[51]

2.3. Pt–Ni–Co Alloys

Pt–Ni–Co systems were described as stable and active ORR electrocatalysts and present a well-investigated group of trimetallic Pt-based catalysts.^[52,53] Zhao et al. found

for optimized PtNi_{0.55}Co_{0.1}/C octahedra (2.8 A mg_{Pt}⁻¹) a 14.7 time improvement of MA in comparison to commercial Pt/C (0.19 A mg_{Pt}⁻¹).^[53] Recently, Jiang et al. presented a facile synthesis of uniform Pt-based nanowires, which are very stable and offer an excellent initial activity of 4.20 A mg_{Pt}⁻¹ for the trimetallic Pt–Ni–Co system.^[54] The Pt mass-based activity of PtNiCo outperforms significantly in comparison to Pt/C and their Pt monometallic (1.06 A mg_{Pt}⁻¹) and Pt–Ni bimetallic (2.97 A mg_{Pt}⁻¹) nanowires. A molten salt synthesis was used by Lokanathan et al. to produce ordered Pt₂CoNi alloys with an exceptional ORR activity (0.93 A mg_{Pt}⁻¹) and record-breaking durability after 15 000 (2.81 A mg_{Pt}⁻¹) and 25 000 (2.2 A mg_{Pt}⁻¹) potential cycles. The excellent activities are supported by DFT calculation, suggesting an optimal ratio of d/valance electron and valance center.^[55]

2.4. Pt–Cu and Pt–Fe Alloys

Pt–Cu-based alloys have been widely investigated in terms of their morphology, composition, and size.^[37,56] Monteverde Videla et al. studied the influence of the preparation method of Pt₃Cu particles supported on multiwall carbon nanotubes on the resulting ORR activity. They compared a thermal reduction method, a chemical reduction method, and an alloy method. The best ORR activity was found for the particles obtained by the chemical reduction method, which the author attribute to the lowest average particles size.^[57] Another group reported on the implementation of a second reduction step in the synthesis using NaBH₄ and were able to significantly enhance the Cu content in their nanoparticles.^[58] Sohn et al. systematically investigated the effect of postsynthesis annealing and acid leaching on the resulting catalyst structure and ORR performance.^[59] A PtCu₃ system was also described by Lee et al. who used Cu cores as seeds and deposited a Cu₃Pt shell on top of them. With that excellent ORR and MOR activities were reached which they attribute to the preferentially exposed {111} facets of the Cu₃Pt shell.^[60] Onion-like Pt-terminated Pt–Cu bimetallic electrocatalysts, consisting of a Pt core surrounded by a Pt–Cu alloy layer and a Pt-enriched shell, showed higher ORR activities (0.54 A mg_{Pt}⁻¹) than Pt/C (0.21 A mg_{Pt}⁻¹). In single-cell ADT degradation tests, the particles show superior stability in contrast to Pt/C.^[61]

Trimetallic systems have been compared to their bimetallic counterparts. Pt₃Cu₁₀Ag showed enhanced activity in comparison to the other bi- and trimetallic systems, which have been investigated in a study by Zhou and Zhang.^[62] The same is true for trimetallic Pt–Cu–Ni materials. Li et al. investigated Pt–Cu–Ni trimetallic systems with different compositions in terms of their ORR. They found the best performance for Pt₂₃Cu₅₁Ni₂₆/C with 0.9 A mg_{Pt}⁻¹ which shown a 2× enhancement in comparison to Pt–Cu/C (0.45 A mg_{Pt}⁻¹).^[63]

Just recently it was shown that doping PtCu nanoparticles with Mo leads to 2–4× higher ORR performance and great durability as shown in a microlaminar fuel half-cell. DFT studies suggest that the exceptional electrocatalytic performances can be attributed to the Mo atoms, which are resistant to oxidation.^[64]

PtCu₂ hexapods with dimensions of around 20 nm exhibit the highest ORR activities reported for Pt–Cu alloys (2.4 A mg_{Pt}⁻¹). Li et al. introduced a synthesis protocol allowing the preparation of various Pt/Cu ratios and revealed the growth mechanism of the hexapods.^[65] PtCu octahedral nanoparticles show an excellent ORR activity (1.2 A mg_{Pt}⁻¹), fabricated by a facile one-pot method. Doping with traces of gold lowers its initial activity (1.0 A mg_{Pt}⁻¹) and greatly improves its stability (8% vs 32% loss after 10 000 cycles).^[66]

Chemically ordered Pt–Fe nanoparticles have been mostly described as hard magnetic materials and for data storage.^[67] Earlier studies have shown that the ordered structure is not only more robust against leaching in acid, but also shows enhanced electrocatalytic ORR activity.^[68,69] A heat treatment is necessary in order to transform the disordered face-centered cubic (fcc) structure, obtained after synthesis, to the chemically ordered face-centered tetragonal (fct) structure to unfold the real potential of the Pt–Fe alloy material. During heat treatment at temperatures >500 °C, the challenge is to protect the nanoparticles from aggregation by embedding them in a thermally stable matrix that can easily be removed by washing afterward.^[68,70] There is constant progress in designing new protocols completely converting the disordered structure to the ordered.^[71]

Duan et al. investigated the impact of different ratios of Pt–Fe and found an optimized ORR activity for Pt₇₅Fe₂₅ over Pt₅₅Fe₄₅, PtFe/C, and Pt/C. Their particles were remarkable stable even though they were not supported.^[72] Highly durable and active PtFe nanoparticles were obtained by thermal annealing of polydopamine-coated PtFe NPs. The particles were in situ coated with a 1 nm N-doped carbon shell during annealing which protects the particles from detachment, agglomeration, and dissolution during fuel cell operating conditions. Figure 3e shows the systematic synthesis diagram and an HAADF-STEM image of the carbon-supported and N-doped carbon-coated ordered fct–PtFe nanoparticles. The authors tested their particle in RDE and MEA and found good ORR activities (1.6 A mg_{Pt}⁻¹) and excellent durability in MEA tests for the fct–PtFe/C catalyst. They attribute the good catalytic activity and durability to the formation of an ordered fct–PtFe alloy, which exhibits a narrow distribution of vacancy formation energy, inhibiting the removal of Fe atoms from the catalyst surface.^[73]

Hollow Pt–Fe alloy nanoparticles were prepared by the direct transformation from solid Pt–Fe NPs into hollow Pt–Fe particles with a Pt-skin surface. The hollow particles reached initial MA of 0.99 and 0.72 A mg_{Pt}⁻¹ after 20 000 cycles durability test. DFT calculations suggest a decrease of the d-band center of the Pt shell accompanied by a weakened adsorption of nonreactive oxygen species, which leads to an improvement in ORR activity.^[74]

2.5. Platinum–Rare Earth (Pt–RE) Alloys Including Early Transition Metals (Sc, Y, Zr, and Hf) and Lanthanides (La, Ce, Pr, Sm, Gd, Tb, Dy, and Tm)

Pt–rare earths (RE) including early transition metals (Sc, Y, Zr, and Hf) and lanthanides (La, Ce, Pr, Sm, Gd, Tb, Dy, and Tm) alloys are characterized by a heat of formation (or alloying energy, E_{alloy}) which is much more negative than that of any

Pt-late transition metal alloys such as Pt₃Ni and Pt₃Co.^[75,76] This is expected to improve the stability of these catalysts against degradation by dealloying since E_{alloy} should substantially contribute to the diffusion barrier of RE atoms to the surface of the Pt-RE alloy. Among the Pt-early transition metal alloys, sputter-cleaned polycrystalline electrodes of intermetallic Pt₃Y were found to be the most active.^[76,77] Following these promising results, other intermetallic compounds were investigated, among Pt₅La and several Pt-lanthanides.^[75,78] In a systematic study by Escudero-Escribano et al., Pt₅Tb displayed the initial highest specific activity (SA), while Pt₅Gd showed the highest SA after stability test.^[78] Interestingly, it was found that a Sabatier Volcano-type relation holds for the ORR activity when plotted as a function of the lattice parameter a of the hexagonal crystal structure (Figure 4a). This relation was recently confirmed by Garlyyev et al. showing that Pt₅Pr follows the same trend.^[79] The high ORR activity was proposed to originate from the optimal binding energy for the OH* intermediate caused by compressive strain exerted to the Pt surface by the underlying bulk alloy.^[78] In the last decade some of these materials have been investigated as single crystal,^[80] polycrystalline,^[75,77,78] and sputter-deposited electrodes.^[81] However, only recently a highly promising candidate from this catalyst family was synthesized as nanoparticles with methods suitable for scale-up production to the gram scale^[82] due to a number of formidable challenges in part associated with the high oxophilicity of RE such as Y (and Gd). This and the much more negative standard reduction potential compared to Pt require the formation of the alloy to occur in absolute absence of molecular oxygen, and chemically

bonded oxygen, in particular water. In addition, high temperature might be necessary for structurally ordered intermetallic compounds. Favorable conditions for formation of alloy nanoparticles via a physical method were obtained by Chorkendorff and co-workers.^[83,84] They synthesized nanoparticles of Pt_xY^[83] and Pt_xGd^[84] on planar glassy carbon electrodes using a magnetron sputter gas aggregation source combined with mass filtering under ultrahigh vacuum (UHV) conditions. As for the polycrystalline electrodes, a Pt surface overlayer is formed under operation. The particle size dependence on the activity and stability was investigated (Figure 4b).^[84] While the formation of intermetallic Pt_xRE via other synthesis routes appeared to be very challenging, PtRE alloy nanoparticles with face-centered cubic structure or RE-containing Pt nanoparticle catalysts were synthesized by different chemical methods.^[85] Notably, Kanady et al. synthesized intermetallic Pt₃Y nanoparticles by a solution process using molten borohydride (MEt₃BH, M = Na, K) as both reducing agent and reaction medium but unfortunately their activity for ORR has not been reported yet.^[86] Asen et al. investigated electrochemical deposition of Pt, Y, and La in ionic liquid as preliminary work with the aim of developing a codeposition procedure for Pt-rare earth alloys.^[87] Several challenges were highlighted including competitive passivation reactions, solubility of precursors, and effect of interfacial structure of ionic liquids at the electrode surface on the ions approaching the electrode. Recently, Roy et al. synthesized a carbon-supported intermetallic Pt_xY nanoparticle catalyst using a metal reactor setup for high-temperature synthesis and Pt/C nanoparticles as precursor.^[82] Intermetallic Pt_xY formation was

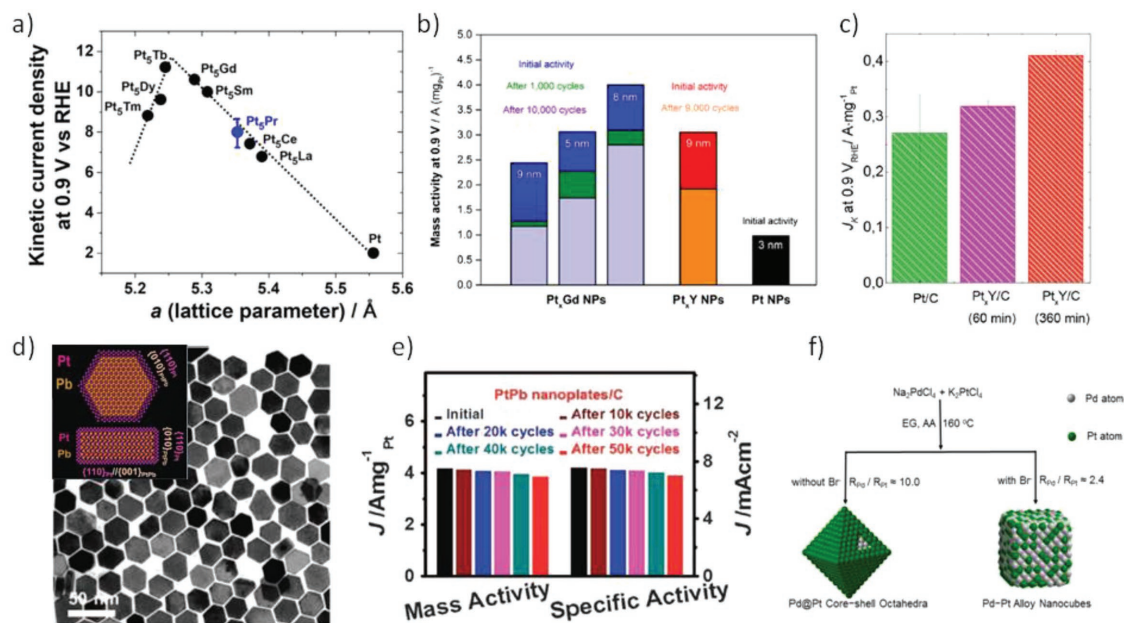


Figure 4. PtRe from polycrystalline electrodes to supported nanoparticles, PtPb intermetallic alloys, and PtPd alloys and core-shell. a) Volcano curves obtained by plotting the kinetic current densities of PtRE polycrystalline electrodes versus their lattice parameters. The data points corresponding to Pt₅Pr (blue)^[79] follow the same trend as the data points (black).^[78] Reproduced with permission.^[79] Copyright 2018, Elsevier. Copyright 2016, AAAS. Copyright 2018, Elsevier. b) Mass activity of Pt₃Gd and Pt₃Y nanoparticles that were deposited on planar GC electrodes. Reproduced with permission.^[84] Copyright 2014, Elsevier. c) Mass activity of carbon-supported Pt₃Y nanoparticles. Reproduced with permission.^[82] Copyright 2018, American Chemical Society. d) TEM image of PtPb hexagonal nanoplates with inset showing the schematic atom models. e) Mass and specific activity changes after different potential cycles for the PtPb nanoplates supported on carbon. d, e) Reproduced with permission.^[91] Copyright 2016, AAAS. f) Scheme showing the role of Br⁻ ions in the formation of Pd@Pt core-shell octahedra and Pd-Pt alloy nanocubes. Reproduced with permission.^[98] Copyright 2016, American Chemical Society.

confirmed by XRD. The most active catalyst showed lower performance than the corresponding Pt_xY catalyst obtained from the magnetron sputter gas aggregation source (Figure 4c). Their catalytic activity was also clearly lower than that of dealloyed or spherical Pt–Co/Ni nanocatalysts. This was suggested to be due to the presence of multiple solid alloy phases rather than a desirable single Pt_3Y phase^[77] combined with a nonoptimal particle size.^[83,84] Nonetheless this study showed for the first time the improved catalytic activity with respect to Pt/C of carbon-supported Pt_xY synthesized in the gram scale.

2.6. Pt–Alkaline Earth (Pt–Ca, Pt–Sr) Alloys

Pt–alkaline earth (Pt–AE) alloys can crystallize in the same intermetallic structure as Pt lanthanides with 5:1 Pt:X stoichiometry (prototype Cu_5Ca) and have similar heat of formation.^[88] Currently, Pt–AE alloys, more specifically Pt_5Ca and Pt_5Sr , have only been investigated as polycrystalline alloys.^[78,88] Both alloys showed very high ORR initial activity, comparable or even higher than Pt_5Gd in the case of Pt_5Sr , while stability was much lower (43% and 49% loss for Pt_5Ca and Pt_5Sr , respectively), which might be due to the slightly lower heat of formation and the leaching of Ca and Sr in the electrolyte.^[88]

2.7. Pt–Pb Alloys

Experiments as well as DFT computations have repeatedly shown that lattice strain of a Pt alloy surface follows a linear relationship with adsorbate chemisorption energy in many Pt alloy systems, and in particular compressive strain weakens the oxygen chemisorption energy for a Pt(111) surface.^[4,89] While this is considered the explanation for the enhanced ORR activity of the Pt–RE and Pt–AE intermetallic catalysts, Bu et al. proposed, supported by DFT calculations, that a large tensile strain is responsible for the high activity of a class of Pt–Pb intermetallic catalysts.^[90,91] They synthesized intermetallic $Pt_{55.9}Pb_{44.1}$ hexagonal nanoplates by a nonaqueous method involving ascorbic acid as the reducing agent.^[91] The nanoplates showed core–shell structure with a Pt–Pb hexagonal phase in the core and a cubic Pt phase in the shell (Figure 4d). A biaxial strain composed of 7.5% tensile strain along [001] and compressive strain along [110] was induced in the Pt surface. Large tensile strain along the [001] direction on the Pt edge as well as bottom and top Pt(110) facets of the Pt shell was predicted by DFT calculations to be responsible for the reported high mass activity of 4.3 A mg_{Pt}^{-1} , which falls in the activity range of octahedrally shaped Pt–Ni ORR electrocatalysts. The stability was also impressive with only a 7.7% loss after 50 000 voltage cycles (Figure 4e). In a follow-up work, morphology transitions from hexagonal nanoplates to octahedral nanoparticles were demonstrated by varying the amount of ascorbic acid.^[90] In the same work, the authors also reported on a novel ternary PtPbNi octahedral nanoparticle catalyst with a core–shell structure where Ni was present at the surface forming a PtNi shell on the outside of the intermetallic PtPb core. The best performing sample, $PtPb_{1.12}Ni_{0.14}/C$, achieved an MA of 1.92 A mg_{Pt}^{-1} which was superior than other binary PtPb octahedral nanoparticles

prepared with the same method, and 17.2% activity loss after 15 000 cycles. Another class of intermetallic PtPb nanoparticles was reported by Matsumoto and co-workers.^[92] Upon potential cycling, the ordered intermetallic PtPb phase changed to a Pt_3Pb phase due to dealloying of Pb. The Pt_3Pb phase was found more active than the initial phase, while further cycling induced the creation of a Pt shell on top of the Pt_3Pb phase which reduced the activity.

2.8. Pt–Pd Alloys

Well-alloyed disordered Pt–Pd alloys as well as Pt–Pd core–shell structures were investigated as ORR electrocatalysts, including shape-selected Pt–Pd nanoparticles.^[93–100] Pd is less expensive than Pt, crystallizes in the same fcc structure, and has similar but slightly smaller lattice constant. However, Pd leaches in the harsh environment of ORR much more readily, therefore the formation of a Pt shell has been often envisaged as a way to protect the Pd alloy core. On the contrary, in recent approaches targeting nanocage and nanoframe structures, the Pd core is intentionally leached to give access to the internal Pt surface of the Pt shell.^[101] Xia and co-workers demonstrated Pd@Pt core–shell octahedral nanoparticles with variable Pt shell thickness from 2 to 5 atomic layers using impressive scanning transmission electron microscopy images and elemental mappings.^[96,99] They compared a polyol-based route and a water-based route, where Pd seeds are formed in a first step and then the Pt shell is grown in a second step.^[99] The enhancement with respect to Pt/C nanoparticles was explained using DFT calculations that revealed destabilization of the OH_{ads} on the Pt/Pd(111) surface simulating the surface of the core–shell nanoparticles with respect to Pt(111). Both ligand effects and lattice strain effects were suggested to play an important role. In the follow-up work, a one-pot synthesis was investigated by the same group.^[98] By controlling the amount of KBr either Pd core–Pt shell octahedral or PtPd cubic nanoparticles could be obtained (Figure 4f). The Pd@Pt octahedra showed the higher MA activity, 1.05 A mg_{Pt}^{-1} , surpassing the previous performance.^[99] A poly(vinyl pyrrolidone) (PVP)-free synthesis method was also investigated.^[93] The durability of this class Pd@Pt octahedra was systematically investigated in a following work.^[96] Formation of hollow structures by leaching of Pd core was observed after 10 000 potential cycles, at which point the mass activity reached its maximum, 1.40 A mg_{Pt}^{-1} , before decreasing with further potential cycling. While most of the cited octahedral core–shell structure works are based on a single element Pd core, multielement PdX alloy cores are also under investigation. Liu et al. reported a core–shell nanoparticle catalyst with a ternary Pd_6CoCu core and a Pt shell that showed an initial MA of 1.46 A mg_{Pt}^{-1} .^[95] The Pt shell was obtained by spontaneous displacement on a thin Pd rich shell formed on the as-prepared Pd_6CoCu core. A different design of multielement PtPd-based catalyst was adopted by Cho et al.^[94] They synthesized octahedral core–shell $Pt_{42.6}Pd_{55.9}Mo_{1.5}$ nanoparticles with the structure consisting in a Mo-doped Pt shell on binary PtPd core. When the nanoparticles were supported on ionic block copolymer-functionalized reduced graphene oxide (IG) a very high MA of 2.46 A mg_{Pt}^{-1} was measured.

Promising durability of the Mo-doped PdPt@Pt/IG catalyst was also shown by performing advance degradation test. The effect on the ORR catalytic activity of a class of alloy nanoparticles with various Pt–Pd bimetallic composition was investigated by Wu et al. combining electrochemistry, DFT calculations, and pair distribution function analysis of high-energy X-ray diffraction patterns obtained at synchrotron.^[97] The maximum ORR activity was obtained for Pt:Pd ratio of 10:90.

3. Cu-Based Nanoalloys for the Carbon Dioxide Reduction Reaction

The elemental metallic electrochemical CO₂ reduction catalysts are traditionally classified into four distinct groups depending on the main chemical reaction product, either formic acid, CO, hydrogen, or hydrocarbons, they generate in experiments. Figure 5a shows a portion of the periodic table containing elements that catalyze CO₂RR with significant Faradaic efficiencies with respect to the four major products.^[102,103] Recently, based on density functional theory calculations, a theoretical justification and explanation was provided for the four groups. Calculations indicated that the chemisorption of atomic hydrogen provides a suitable descriptor of the experimentally observed Faradaic efficiency, the chemisorption energy of CO determines whether the catalyst generates CO or “beyond CO” products, while the chemisorption of the COOH intermediate controls the onset potential of the CO₂RR process. Figure 5b reports the difference between H* chemisorption and *COOH chemisorption as a function of the H* chemisorption energy. In the plot the four major groups of elemental CO₂RR catalyst clearly unfold along the x-axis. Figure 5c demonstrates how the experimentally achieved Faradaic efficiency follows almost linearly the H* chemisorption. Clearly, the more unstable the atomic hydrogen atom is, the larger the kinetic barrier for the competing hydrogen evolution process and the more selective the formation of carbonaceous products during the CO₂RR.^[103]

Copper (Cu) has attracted the most attention as a catalyst to produce hydrocarbons^[104] because Cu is the only metal that uniquely binds CO neither too strong nor too weak on the catalyst surface for further reduction into several hydrocarbons. Indium (In), tin (Sn), and lead (Pb) metals are known to mainly generate formate/formic acid in the electrochemical CO₂RR. In

addition, these metals could largely suppress the competitive hydrogen evolution reaction.^[105] Bagger et al. showed that the formic acid producing metals have no, if not negligible, amount of hydrogen adsorbed at relevant potentials. Zinc (Zn) as well as precious metals gold (Au) and silver (Ag) are well known for their preferential production of CO from the electrochemical reduction of CO₂.^[106] This behavior originates from their relatively low binding strength to *CO, which is readily released from the surface, denying any further reduction.^[103] The production of CO from the electrochemical CO₂RR is arguably the technologically most advanced and commercially most promising reaction pathway due to the mechanistic simplicity compared to the formation of dimerization products. While this simplicity enables a relatively high selectivity for the CO evolution, the high cost of the precious metal catalyst is limiting widespread application.^[107] On the other hand, in the case of platinum (Pt), nickel (Ni), and palladium (Pd), it is well known that hydrogen under potential deposition (H_{upd}) and the kinetically facile hydrogen evolution reaction are a consequence of the strong binding of atomic hydrogen on the catalyst surface. As a result of this, the low chemical selectivity, catalytic CO₂RR activity, and excessive hydrogen gas generation have remained fundamental challenges of these elements when used as CO₂RR catalysts.

One of the strategies to address these selectivity and activity issues is designing electrocatalysts by combining one metal with another, i.e., alloys, rather than single elemental metals. The various nanoalloy catalysts have been developed and applied to electrochemical CO₂RR,^[108] and we address recent progress on Cu-based alloy catalysts with formate-producing metals (In and Sn), CO-producing metals (Au, Ag, and Zn), and H₂-producing metals (Pd and Pt) in the following sections. We summarize this section with a discussion of tunable activity and selectivity of the CO₂RR catalyzed by these materials.

3.1. Cu–In/Sn Alloys

This section covers Cu-based alloy catalysts incorporating formate-producing metals as a promising strategy in electrochemical CO₂ reduction. We show why the combination of copper with other metals can show different reactivity and selectivity through synergistic effects such as bifunctional, geometric, and electronic structure changes.

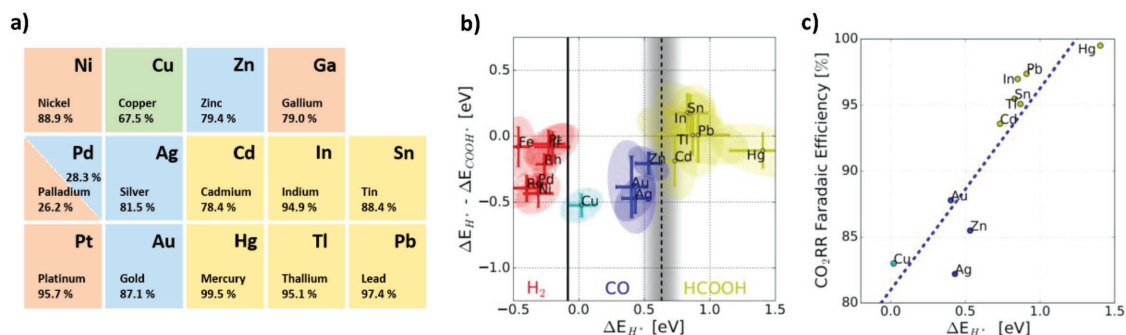


Figure 5. Classification of various metal depending on formation of major products in electrochemical CO₂ reduction. a) Periodic table and Faradaic efficiency of major product from experimental data by Hori.^[102] H₂ (red), CO (blue), formate (yellow), hydrocarbon (green). b) The experimental product classification of H₂, CO, and HCOOH by the $\Delta E_{H^*} - \Delta E_{CO_2H^*}$ and the ΔE_{H^*} . c) Faradaic efficiency of CO₂ reduction reaction by ΔE_{H^*} . a–c) Adapted with permission.^[103] Copyright 2017, John Wiley and Sons.

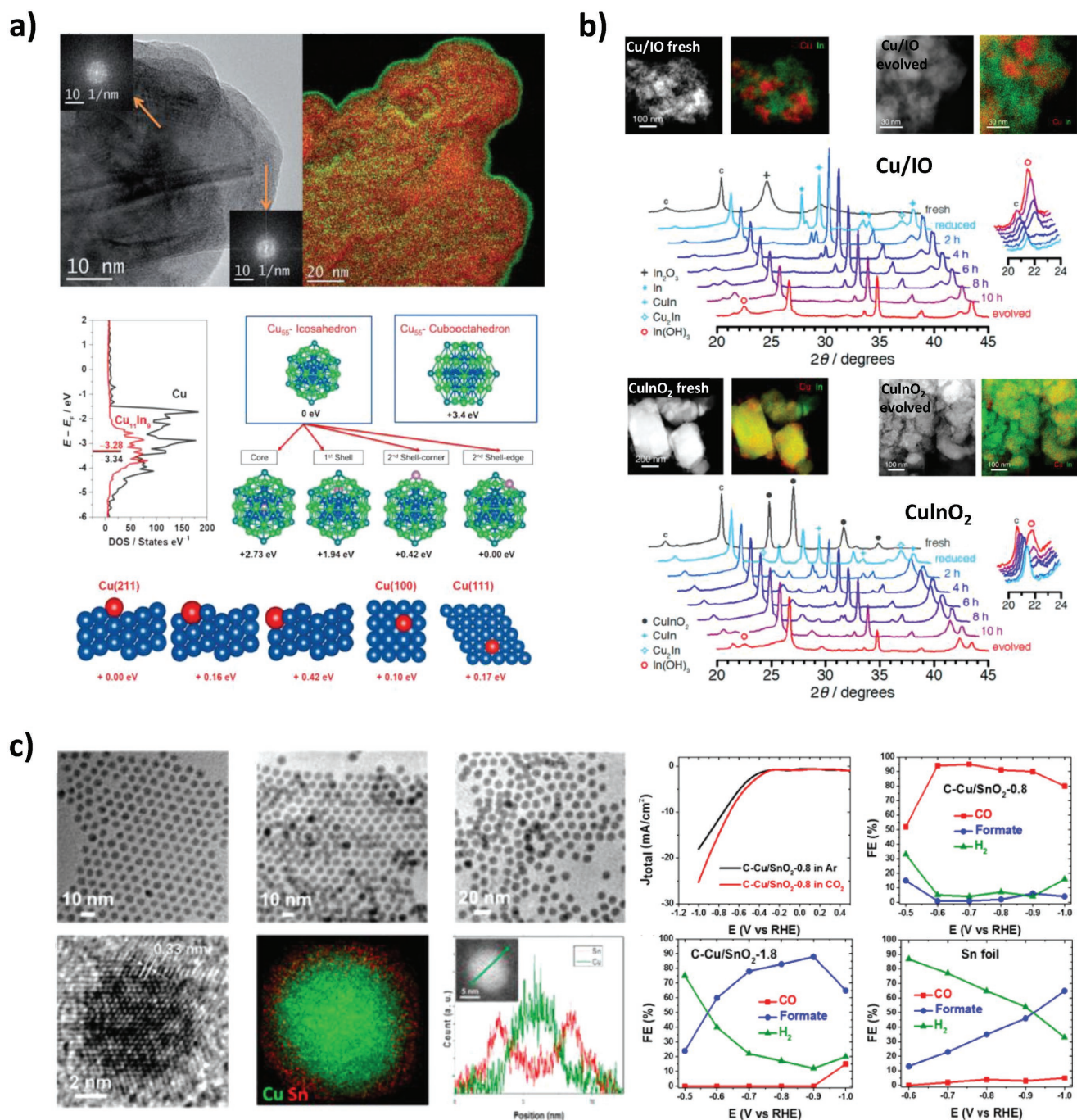


Figure 6. Core@shell structure of various Cu-based bimetallic catalysts. a) HR-TEM images and DFT calculation of Cu-In alloy. Reproduced with permission.^[109] Copyright 2015, Wiley-VCH. b) HAADF-STEM images and XRD pattern of Cu-rich@In(OH)₃ from CuInO₂- and In₂O₃-supported Cu nanoparticles. Reproduced with permission.^[111] Copyright 2016, American Chemical Society. c) TEM image of Cu@SnO₂ with difference thickness and its electrochemical CO₂ reduction. Reproduced with permission.^[114] Copyright 2017, American Chemical Society.

3.1.1. Cu-In

Copper-indium alloys were repeatedly proposed as promising CO₂ reduction catalyst systems. Cu-In alloy electrodes were prepared by electrodeposition, electrochemical reduction, and chemical reduction. Rasul et al. reported a Cu-In alloy catalyst synthesized by electrochemical deposition on the oxide-derived

Cu (OD-Cu), which showed 95% CO Faradic efficiency in electrochemical CO₂ reduction (Figure 6a).^[109] Although In does not have a significant effect on the Cu electronic structure, DFT calculations show that In atoms, which preferentially located on the edge sites, affected the adsorption properties of neighboring Cu terrace atoms, which in turn inhibited H adsorption. In a subsequent study, the authors reported Cu-In alloys

that consisted of bimetallic Cu₁₁In₉, Cu₇In₃ and Cu by using a unique generation method of electrochemical reduction of mixed metal oxide, CuInO₂.^[110] These alloys showed a higher CO₂ conversion to HCOOH and CO, wherein H₂ Faradaic efficiency remained under 10%.

Cu-rich core–In(OH)₃ shell nanostructures were also derived from over several electrochemical cycling of CuInO₂ and In₂O₃-supported Cu nanoparticles (Figure 6b).^[111] The evolved Cu–In(OH)₃ core–shell catalyst exhibited high CO yield, indicating that In(OH)₃ has a crucial role in CO selectivity for CO₂RR. Recently, Hoffman et al. investigated electrodeposited dendritic Cu–In alloys of various compositions and their electrocatalytic CO₂ reduction activity.^[112] At 40 at% indium, high formate was produced at –1.0 V_{RHE}, and an optimal syngas ratio was obtained. Furthermore, maximum of 62% formate Faradaic efficient was obtained at 80 at% indium.

3.1.2. Cu–Sn

Tin is also a metal that strongly inhibits hydrogen generation through low chemisorption energies, and this is why Cu–Sn alloys attracted attention as efficient CO₂RR catalysts. Sarfraz et al. reported Cu–Sn bimetal catalyst that was prepared by electrodeposition of Sn on the OD-Cu. This electrode exhibits high selectivity and stability of over 90% CO Faradaic efficiency for 14 h at –0.6 V_{RHE}.^[113] The authors claimed similar geometric effects to Cu–In bimetal catalyst through DFT calculation and suggested that replacing a single atom with a Sn atom at a specific site can destabilize H adsorption to inhibit H₂ formation while CO binding sites were mostly unchanged. Recently, Cu@SnO₂ core–shell nanostructure catalysts synthesized by a seed-mediated method in wet chemistry (Figure 6c) were reported.^[114] Li et al. suggested that a thin layer of SnO₂-coated Cu nanoparticles has tunable activity and selectivity depending on Sn thickness in electrochemical CO₂ reduction. The thicker Cu@SnO₂ shell (1.8 nm) behaves more Sn-like in activity to produce formate while a thinner Cu@SnO₂ shell (0.8 nm) shows high CO activity and selectivity, resulting in 93% Faradaic efficiency at –0.7 V_{RHE}. Theoretically, they suggested that the thin layer shell of SnO₂ is likely an alloy with Cu, forming a uniaxially compressed SnO₂ lattice for enhanced CO production, which indicates a change in electronic structure.

3.2. Cu–Au/Ag/Zn Alloys

Alloying CO-selective metals with Cu constitutes a promising approach to reduce material cost for CO catalysts while achieving higher catalytic activities. Also, studies on segregated bimetallic catalysts consisting of a CO-producing metal with Cu allowed the analysis of interesting fundamental bifunctional effects, such as intermetallic CO spillover.

3.2.1. Cu–Au

The most intensively studied bimetallic system is the Au–Cu one. This is, in part, because the Cu–Au forms well defined face-centered ordered and disordered alloys. Initial studies

mainly focused on the production of bimetallic systems by galvanic displacement, bulk mixtures of metal melts,^[115] and electrochemical deposition.^[116] While the increase in Au content usually resulted in a catalytic signature strongly reminiscent of pure Au, some compositions showed enhanced productions of C₂H₄,^[117] CO,^[115] and even alcohols.^[116] Christophe et al. suggested an accelerated desorption of *CO from the gold sites, which they proposed is induced by dipole–dipole repulsion due to neighboring *CO bound to Cu sites, to be the origin of enhanced CO production on the Au/Cu system.^[115] For multi-metal systems, structural stability is an important parameter to consider as dynamic phase changes can readily occur, especially under applied potentials and in the presence of reactive gases. Friebel et al. have investigated the properties of Cu overlayers on a gold substrate using in situ XAS in an alkaline electrolyte. While a 12.5% expansion of the Cu lattice could be initially observed in the Cu overlayer, an applied potential resulted in the formation of a Au-rich surface alloy.^[118] This study is in line with a DFT-based investigation of Lysgaard et al., who discussed the stability of nanoalloys on the model of a bimetallic icosahedral composed of 309 atoms. Their simulation shows the segregation of phases into a Cu-rich core and a Au-rich shell due to the difference in atomic size of the two metals.^[119] Recent experimental studies on atomic ordering^[120] and size–reactivity relationship of Au/Cu particles^[121] propose a segregation of Au from Au/Cu alloys to the surface and discuss effects of compressive strain and the presence of undercoordinated sites as the origin of enhanced CO₂RR activity. The effect of strain is further discussed in a related study by Monzó et al. who have observed that an increasing layer thickness of Cu on a Au core was enhancing the protonation pathway, favoring H₂ and CH₄ production at the cost of ethylene.^[122] Next to strain, geometric and electronic alterations are also important parameters proposed to alter catalyst reactivity. Kim et al. varied the Au/Cu ratio of spherical particles with a diameter of roughly 10 nm to investigate the influence of electronic effects on the CO₂RR activity (Figure 7a). While confirming the formation of an alloy via XRD and surface plasmon resonance (SPR), they observed a rising Faradaic efficiency for CO with increasing Au ratio, whereas other gaseous products were diminishing. They monitored the shift of the d-band center with varying metal ratios by XPS, which showed a decrease with higher Au content, agreeing with the witnessed change in product distribution. Interestingly, the Au₃Cu differed from the trend and showed the highest CO mass activity. This deviation was suggested to be caused by a geometric effect, stabilizing the *COOH intermediate by simultaneously binding the C-end through a Au-atom and the O-end through a neighboring Cu atom.^[123] This result is similar to what Christophe et al. observed earlier, even though they suggested weaker *CO binding to be the cause of the improvement, highlighting the importance of geometric arrangements.

3.2.2. Cu–Ag

Distinct analogies to the Cu–Au system are apparent in the Ag–Cu system as well. Chang et al. synthesized particles composed of Cu overlayers of varying thickness on a silver core. They could observe an increased CO production for silver-rich

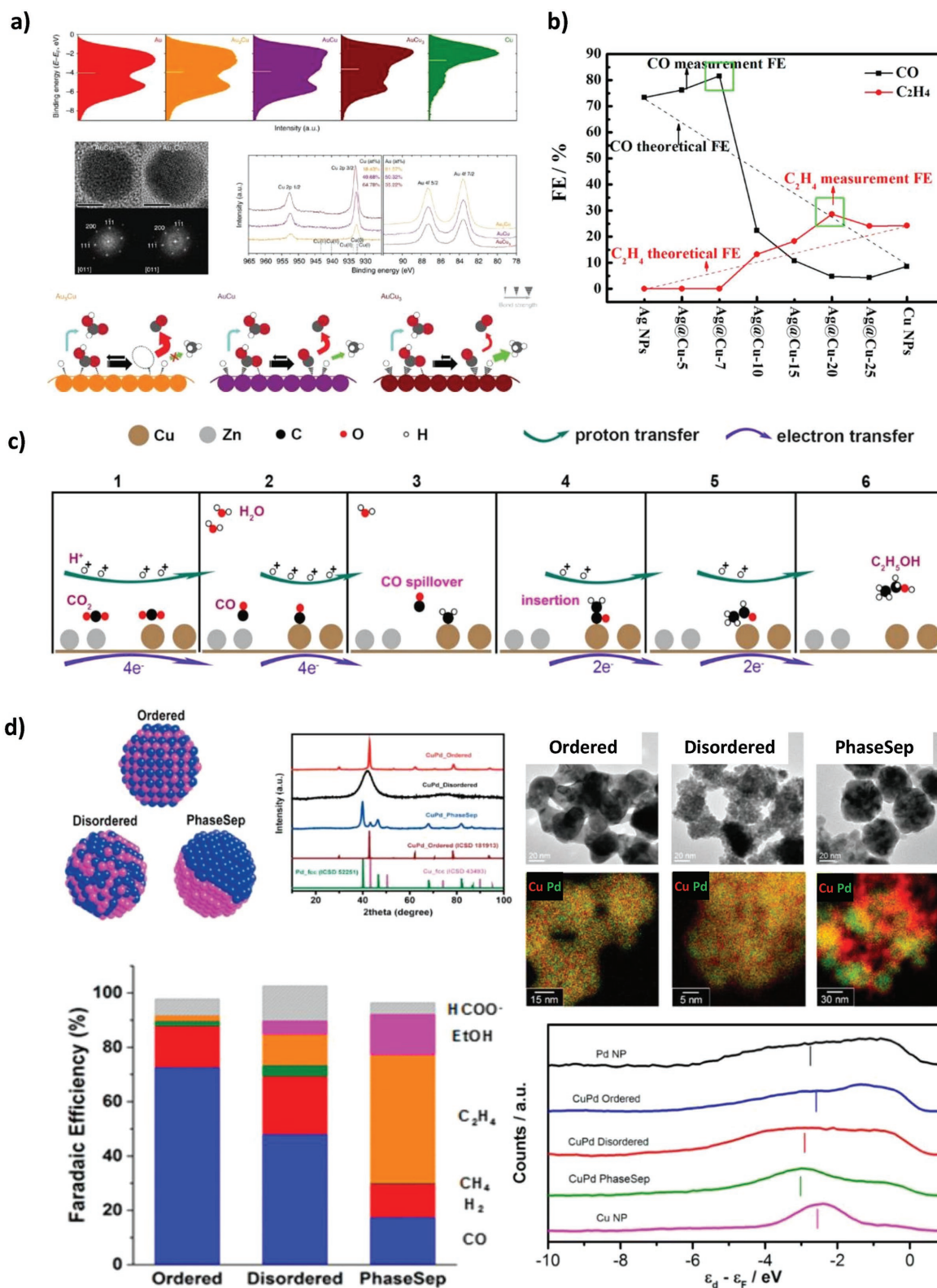


Figure 7. Cu-based bimetallic catalysts showing various alloying effects. a) Influence of variation in Cu/Au ratio on the surface valence band. Reproduced with permission.^[123] Copyright 2014, Springer Nature. b) Change in CO₂RR selectivity with increasing Cu overlayer thickness on Ag particles. Reproduced with permission.^[124] Copyright 2017, American Chemical Society. c) Proposed “CO-spillover” mechanism for a Cu/Zn system. Reproduced with permission.^[126] Copyright 2016, American Chemical Society. d) The geometric effect from atom arrangement in the Cu–Pd system. Reproduced with permission.^[138] Copyright 2017, American Chemical Society.

particles and an enhanced ethylene formation for copper-rich particles with respect to the monometallic cases, and claimed those “synergistic” effects to originate in the geometric distribution. A stronger CO binding caused by Cu-lattice expansion on the Ag substrate is suggested to enhance the ethylene formation, while the presence of oxygen-affine metals as copper is believed to stabilize *COOH, favoring CO formation in the silver-rich case (Figure 7b).^[124] In contrast, Bell and co-workers studied a Ag/Cu alloy, which showed surface enrichment in Cu under applied electrode potential. Here, the resulting Cu-rich surface was proposed to be compressively strained, lowering the binding of *H and *O. An observed increase in the formation of oxygenated products at the expense of hydrogen and hydrocarbons was suggested to be the result of reduced amounts of adsorbed *H, limiting the cleavage of the C–O bond.^[125] Noteworthy, there are some studies proposing a remarkable effect of alloying, suggesting a two-site mechanism in which one metal, as in Zn or Ag, is producing CO, which can be further reduced at neighboring Cu sites.^[126,127] For the case of Ag, Hoang et al. deposited Cu/Ag wires on a carbon paper substrate. While EXAFS results were suggesting an alloy formation, the relatively low content of 6% Ag showed a strong beneficial effect for ethylene selectivity, achieving almost 60%. They claimed this enhanced ethylene selectivity originates first from Ag stabilizing the Cu₂O phase, as well as from Ag acting as a CO source, which can locally enhance the reactant concentration.^[127]

3.2.3. Cu–Zn

Most studies on the Cu–Zn catalyst system report a high selectivity for 2e[−] transfer products such as CO. After alloying with Cu, a “two-site” catalyst was claimed to form, where Zn site served as CO producer and adjacent Cu site for further reduction.^[128] Ren et al. electrodeposited Cu/Zn films and showed remarkably high Faradaic efficiency of up to 29% for ethanol. This exceptional selectivity for ethanol was suggested to origin from a spillover of CO, which is produced at Zn sites and further reduced at Cu sites (Figure 7c). It is striking, however, that no similar observations were made in other studies of the Zn/Cu system suggesting the geometric arrangement of the active sites to be of utmost importance for the observed effect.^[126]

3.3. Cu–Pd/Pt Alloys

Cu alloys, which contain group VIII metals such as Pt and Pd, have been under much investigation as CO₂RR catalysts. The competition between CO₂RR and HER is controlled by the chemisorption of the key intermediates during the reactions, i.e., *CO in CO₂RR and *H in HER. Although Pt and Pd adsorb atomic hydrogen readily more positive of the thermodynamic standard potentials, and therefore present relatively low kinetic barriers and overpotentials for the HER,^[129] the copresence of *CO can actually suppress the absorption of *H.^[130] Compared to Pt, Pd plays a somewhat special role due to its unique property of absorbing hydrogen atoms in its bulk structure. It is known to exhibit high selectivity toward CO and formate

due to the lower adsorption affinity of *CO intermediates, which could also act as a catalytic self-poisoning species during CO₂RR.^[131,132] The surface palladium hydride (PdH_x) phase is considered to be an active phase for formate formation.^[132,133]

3.3.1. Cu–Pd

By alloying Cu with Pd, the chemisorption strength of intermediates on the catalyst surface can be tuned thanks to geometric and electronic effects, enabling an optimal activity and selectivity toward CO₂RR. Li et al. reported a well-defined mesoporous Pd–Cu alloy with Faradaic efficiencies of CO, FE_{CO}, exceeding 80% on Pd–Cu alloy at −0.8 V_{RHE}.^[134] The charge density is altered in Pd–Cu alloy structure compared to the single component. Pd, which serves as an electron donor, was suggested to provide the active sites for the electron acceptors such as COOH* and more favorable for CO desorption in the presence of Cu. On the other hand, Cu atoms only contribute to the activity by affecting the electronic structure of their neighboring Pd atoms and adjust the surface atoms construction. Moreover, the larger surface area created by mesoporous structure provides more active sites for CO₂RR. Yin et al. suggested that the undercoordinated step or adatom sites could be another reason for highly selective CO production on Pd–Cu alloy catalyst.^[135] The tunable size and composition of the bimetallic nanoparticles are crucial to CO₂RR activity and CO selectivity. Pd–Cu alloy with a smaller particle size of 5 nm and a Pd to Cu ratio of 85–15 could significantly improve the catalyst performance, which is further explained by the CO binding energy on the catalyst surface.

The difference in lattice constant between Cu and Pd causes lattice strain effects, exacerbating differences in CO₂RR performance.^[136,137] Zhu et al. developed a facile synthesis route for Pd–Cu bimetallic nanoparticles with various structures.^[136] The concave rhombic dodecahedral with exposed high-index facets exhibits an enhanced CH₄ current density compared to Cu foil, while the flower-like Pd₃Cu shows high FE_{CO} in a wide overpotential range (−0.7 to 1.3 V_{RHE}). A very different selectivity toward C₁ and C₂ products in CO₂RR is also observed by Ma et al. on three Cu–Pd mixing patterns, namely ordered, disordered, and phase-separated (Figure 7d).^[138] The ordered Cu–Pd (Cu:Pd = 1:1) catalyst shows the highest C₁ selectivity (over 80%), while the sample with the same Cu–Pd content but alternating Cu–Pd arrangement favors CH₄ formation, indicating a geometric effect, rather than an electronic effect, seems to be the key factor to determine the selectivity of bimetallic Cu–Pd catalysts. The phase-separated pattern behaved quite differently on ordered and disordered catalysts, where it achieved higher C₂ selectivity (over 60%). The main reason for this is believed to be the geometrically phase-separated system, where the Cu-rich sites are suitable for *CO generation and C–C coupling while the adjacent Pd-rich side attracts sufficient protons for further protonation step. This observation is in agreement with previously reported “two-site” mechanism on Cu–Ag^[127] and Cu–Zn^[128] systems. On the other hand, unlike Cu–Pd catalysts in which Pd participates in catalysis to change the activity and selectivity, Weng et al. reported that Pd atom induces continuous morphological and compositional

restructuring of the Cu surface to clean the Cu surface during the electrolysis and shows high durability of CO₂ reduction to hydrocarbons.^[139]

Cu–Pd alloys could also be coupled with organic molecules or carbon supporters, serving as dual catalysts.^[140] Liu et al. dispersed Cu–Pd alloys on graphene homogeneously.^[141] Compared to monometallic Cu/graphene catalyst, bimetallic Cu–Pd/graphene catalyst shows higher CO₂RR activity, mainly attributed to the higher electrical conductivity of the increased graphitic carbon content. Yang et al. developed a pyridine (PYD) immobilized Cu–Pd catalyst.^[142] It produces 26% methanol and 12% ethanol Faradaic efficiencies, respectively. They claimed that the PYD in the catalyst favors methanol production while Cu component facilitates the generation of ethanol. This bifunctional catalyst also shows remarkable stability over 14 h.

3.3.2. Cu–Pt Alloys as CO₂RR Electrocatalysts

The high activity for the competing HER process and strong CO binding on Pt have restricted applications of Cu–Pt alloys as CO₂RR catalysts.^[143] So far, only a few examples have been investigated. The Cu–Pt catalyst with an optimized atomic molar ratio of 3:1 (Cu:Pt) reported by Guo et al. improves CH₄ formation in 0.5 M KHCO₃.^[144] The key step for CH₄ formation is the protonation of adsorbed *CO. While a high atomic Cu content in Cu–Pt alloy catalyst surfaces increase the effective *CO surface coverage, the atomic proximity of proton-affine Pt surface sites should in theory facilitate the protonation process of *CO to *CHO. However, the strong interaction between Pt and both *CO and H* slows down the protonation. Also, the strong binding of *CO causes Pt surface segregation resulting in a Pt shell characterized by a reactivity similar to pure Pt; therefore, empirically, Cu–Pt catalyst has largely favored the HER process over the CO₂RR after some transient period.

4. Concluding Future Perspectives on Nanoalloys

We have reviewed recent progress and the current state of research on alloy nanocatalysts for the ORR and the CO₂RR processes. Both electrochemical processes proceed within electrode potential ranges where Pt-based and Cu-based alloys, respectively, remain largely metallic in bulk and surface. Clearly, atomic proximity of two dissimilar metal atoms at the surface and in bulk remains one of the most important strategies to modify the interfacial reactivity of metallic surfaces. Phenomena such as surface segregation, bulk alloy ordering, surface spinodal demixing and island formation, or shape-control effects will continue to play important roles in the discovery of novel bimetallic alloy catalysts at the nanoscale.

4.1. Pt-Based Nanoalloy Catalysts for the ORR

Compositional and morphological tuning of Pt-based nanoalloys has resulted in remarkable performance increases over conventional pure Pt nanoparticles during the past decade.

More specifically, using electrode environments suitable for activity screening, shape-selected octahedral Pt–Ni particles as well as roughened Pt–Ni surfaces of leached bimetallic nanowires have demonstrated double digit improvements in ORR Pt mass activity and have generally by large surpassed published technology activity targets for hydrogen–oxygen/air fuel cells, such as Pt mass activity. What remained somewhat of a puzzle about bimetallic Pt nanoalloy ORR catalysts, however, was the fact that compositionally uniform and structurally ordered Pt–Ni nanoalloys, such as well-defined alloy octahedra or cubes, showed comparably high catalytic ORR activities as morphologically, compositionally, and structurally very disordered, nonuniform nanoalloys, such as hollow spheres, octahedra with concave facets, corrugated dealloyed Pt–Ni nanowires or highly porous unsupported PtNi aerogels.^[145] Recently, progress was achieved on this issue by realizing that morphologically and structurally highly disordered alloy particles feature a wide distribution of surface sites on their rough solid surface, which includes Pt surface atoms with a concave local atomic coordination, such as Pt atoms at the bottom of a surface pit, at the bottom of a surface step, or Pt atoms exposed at concavely shaped facets of corrosively degraded Pt alloy octahedra. Computational studies predicted that such concave-type coordinated Pt surface atoms exhibit higher generalized coordination numbers and significantly larger ORR activity, which, on average, makes the disordered structures perform as active as the ideal ordered nanoalloys.^[146] While a reliable experimental quantification of Pt surface atoms with concave coordination has remained a challenge, an experimentally accessible descriptor to quantify the degree of local structural disorder, referred to as surface distortion, was recently put forward.^[145]

A major current challenge of highly active Pt-based nanoalloys catalysts relates to the translation from extremely thin powder catalyst film tests (tens of nanometer thick films, and a few micrograms Pt per cm² electrode area) to thicker electrode layer formats (several tens of micrometers with hundreds of microgram Pt per cm² electrode area), such as typically used in a membrane electrode assembly of a fuel cell stack, *without* any loss in their high catalytic Pt mass activity. Despite much recent effort, the generation of highly active electrode layers in real MEAs using advanced nanoalloy catalysts has remained unsuccessful. This is because there are many conditions to consider in the actual MEA, unlike the ORR in the RDE test. Recently, floating electrode experiments have been introduced considering mass transfer.^[147] We expect to be able to measure the ORR activity in the MEA more accurately through the floating electrode experiment. In the absence of MEAs with optimal activity performance, performance stability data of advanced Pt nanoalloys in MEA layers have remained unknown either. Current challenges involve the prevention of electrochemical leaching of the less noble alloy component, which results in lowering of the proton conductivity of the ionomer in electrode layer and membrane. Again, limited performance losses reported in RDE tests are no reliable predictor for the catalytic performance and stability in MEA formats. Nonetheless, an acid-leached Pt-rich Pt–Co nanoalloy has been incorporated as cathode electrocatalyst in the “Mira” hydrogen fuel cell vehicle commercialized by the Toyota Motor Company. More advanced Pt-based nanoalloys will likely be deployed in the next generations of hydrogen fuel cell vehicle stacks.

4.2. Cu-Based Nanoalloy Catalysts for CO₂RR

Cu surfaces are uniquely reactive catalysts for the CO₂RR due to their broad spectrum of “beyond CO” hydrocarbon and oxygenate reaction products. Structure sensitivity of pure Cu surface has been well studied and led to the discovery of the unique reactivity of {100} facets toward ethylene, which resulted in heightened interests in Cu nanocube catalysts. Cu-based alloys represent a diverse family of CO₂RR, the structure sensitivity of which is large unexplored. A large majority of Cu-based alloys in CO₂RR have proved to favor chemical reduction products of two-electron transfer processed, which suggests that the chemisorption of intermediates of Cu surfaces is masked by minute amounts of dopant dissimilar metal atom in the surface. Another challenge relates to the time stability of activity and selectivity. Faradaic efficiencies evolve over the first few hours of catalysis and, in most cases, the competing hydrogen evolution reaction outperforms the CO₂RR processed due to deposition of metal ion contaminants in the electrolyte which boost hydrogen evolution.

Similar to the Pt nanoalloy world, a majority of catalyst studies are performed in H-cell screening cells that suffer from massive CO₂ mass transport losses at the electrode interface. These mass transfer limitations are often cited as a barrier for projections to large-scale CO₂ electrolyzer performances. To address this problem, a gas diffusion layer-based gas–liquid flow electrolyzer cell proved most suitable to test novel Cu alloys under conditions relevant for commercial-scale electrochemical reactors. The continuously circulated gas and liquid flows in electrolysis flow cell reactors, moving reactants and products to and away from the reactive interfaces and electrodes, help break the mass transport limitations. Therefore, future investigations of new Cu-based nanoalloys, perhaps of all CO₂RR catalysts, should focus on multilayer gas–liquid flow cells.

Looking beyond Cu-based nanoalloys for the CO₂RR, metal–nitrogen-doped high surface carbon catalysts, referred to as MNC electrocatalysts in literature, have emerged as alternative cost-efficient, highly active and selective CO₂RR electrocatalyst for CO production and the generation of “beyond CO” products. In particular, NiNC was reported as highly active and selective CO-producing electrocatalyst rivaling and surpassing the efficiency of Ag or Au catalysts. In addition, MNC catalysts with sufficient chemisorption strength of the *CO intermediates, such as M = Fe, Co, or Mn, allow for CO protonation and formation of methane. Current challenges involve the synthetic preparation of bimetallic M₁–M₂NC nitrogen-doped carbons that could enable the production of C₂ products such as ethylene.

Acknowledgements

This work was funded by the German Federal Ministry of Education and Research (Bundesministerium für Bildung und Forschung, BMBF) under Grant Nos. 03SF0523A (“CO₂EKAT”), 033RC004E (“eEthylene”), and 03SF0527A (“LOPLAKAT”).

Conflict of Interest

The authors declare no conflict of interest.

Keywords

CO₂RR, Cu-based, electrocatalysts, nanoalloys, ORR, Pt-based

Received: August 29, 2018

Revised: October 18, 2018

Published online:

- [1] a) J. A. Turner, *Science* **1999**, *285*, 687; b) C. N. Waters, J. Zalasiewicz, C. Summerhayes, A. D. Barnosky, C. Poirier, A. Gałuszka, A. Cearreta, M. Edgeworth, E. C. Ellis, M. Ellis, C. Jeandel, R. Leinfelder, J. R. McNeill, D. d. Richter, W. Steffen, J. Syvitski, D. Vidas, M. Wagreich, M. Williams, A. Zhisheng, J. Grinevald, E. Odada, N. Oreskes, A. P. Wolfe, *Science* **2016**, *351*, aad2622.
- [2] G. Centi, E. A. Quadrelli, S. Perathoner, *Energy Environ. Sci.* **2013**, *6*, 1711.
- [3] a) B. Roldan Cuenya, *Acc. Chem. Res.* **2013**, *46*, 1682; b) B. R. Cuenya, F. Beharfarid, *Surf. Sci. Rep.* **2015**, *70*, 135; c) M. Ahmadi, H. Mistry, B. Roldan Cuenya, *J. Phys. Chem. Lett.* **2016**, *7*, 3519; d) H. Mistry, A. S. Varela, S. Kühl, P. Strasser, B. R. Cuenya, *Nat. Rev. Mater.* **2016**, *1*, 16009.
- [4] M. Mavrikakis, B. Hammer, J. K. Norskov, *Phys. Rev. Lett.* **1998**, *81*, 2819.
- [5] F. Maroun, F. Ozanam, O. M. Magnussen, R. J. Behm, *Science* **2001**, *293*, 1811.
- [6] S. Martens, L. Asen, G. Ercolano, F. Dionigi, C. Zalitis, A. Hawkins, A. M. Bonastre, L. Seidl, A. C. Knoll, J. Sharman, P. Strasser, D. Jones, O. Schneider, *J. Power Sources* **2018**, *392*, 274.
- [7] a) C. M. Pedersen, M. Escudero-Escribano, A. Velazquez-Palenzuela, L. H. Christensen, I. Chorkendorff, I. E. L. Stephens, *Electrochim. Acta* **2015**, *179*, 647; b) Y. Garsany, J. J. Ge, J. St-Pierre, R. Rocheleau, K. E. Swider-Lyons, *J. Electrochem. Soc.* **2014**, *161*, F628; c) S. S. Kocha, K. Shinozaki, J. W. Zack, D. J. Myers, N. N. Kariuki, T. Nowicki, V. Stamenkovic, Y. J. Kang, D. G. Li, D. Papageorgopoulos, *Electrocatalysis* **2017**, *8*, 366.
- [8] a) C. Wang, M. Chi, G. Wang, D. van der Vliet, D. Li, K. More, H.-H. Wang, J. A. Schlueter, N. M. Markovic, V. R. Stamenkovic, *Adv. Funct. Mater.* **2011**, *21*, 147; b) T. Toda, H. Igarashi, H. Uchida, M. Watanabe, *J. Electrochem. Soc.* **1999**, *146*, 3750; c) V. R. Stamenkovic, B. S. Mun, M. Arenz, K. J. J. Mayrhofer, C. A. Lucas, G. F. Wang, P. N. Ross, N. M. Markovic, *Nat. Mater.* **2007**, *6*, 241; d) S. Mukerjee, S. Srinivasan, M. P. Soriaga, J. McBreen, *J. Phys. Chem.* **1995**, *99*, 4577; e) S. Mukerjee, S. Srinivasan, *J. Electroanal. Chem.* **1993**, *357*, 201; f) K. M. Caldwell, D. E. Ramaker, Q. Jia, S. Mukerjee, J. M. Ziegelbauer, R. S. Kukreja, A. Kongkanand, *J. Phys. Chem. C* **2015**, *119*, 757; g) C. Wang, M. Chi, D. Li, D. Strmcnik, D. van der Vliet, G. Wang, V. Komanicky, K.-C. Chang, A. P. Paulikas, D. Tripkovic, J. Pearson, K. L. More, N. M. Markovic, V. R. Stamenkovic, *J. Am. Chem. Soc.* **2011**, *133*, 14396; h) Y. Kang, J. Snyder, M. Chi, D. Li, K. L. More, N. M. Markovic, V. R. Stamenkovic, *Nano Lett.* **2014**, *14*, 6361; i) S. C. Rudi, C. Cui, L. Gan, P. Strasser, *Electrocatalysis* **2014**, *5*, 408; j) L. Gan, C. Cui, S. Rudi, P. Strasser, *Top. Catal.* **2014**, *57*, 236; k) X. Tuavev, S. Rudi, V. Petkov, A. Hoell, P. Strasser, *ACS Nano* **2013**, *7*, 5666; l) L. Gan, M. Heggen, S. Rudi, P. Strasser, *Nano Lett.* **2012**, *12*, 5423; m) S. Rudi, L. Gan, C. Cui, M. Glicie, P. Strasser, *J. Electrochem. Soc.* **2015**, *162*, F403.
- [9] B.-W. Zhang, Z.-C. Zhang, H.-G. Liao, Y. Gong, L. Gu, X.-M. Qu, L.-X. You, S. Liu, L. Huang, X.-C. Tian, R. Huang, F.-C. Zhu, T. Liu, Y.-X. Jiang, Z.-Y. Zhou, S.-G. Sun, *Nano Energy* **2016**, *19*, 198.

- [10] L. Gan, S. Rudi, C. Cui, M. Heggen, P. Strasser, *Small* **2016**, *12*, 3189.
- [11] Y. Dong, Y.-W. Zhou, M.-Z. Wang, S.-L. Zheng, K. Jiang, W.-B. Cai, *Electrochim. Acta* **2017**, *246*, 242.
- [12] L.-L. Shen, G.-R. Zhang, S. Miao, J. Liu, B.-Q. Xu, *ACS Catal.* **2016**, *6*, 1680.
- [13] a) T. Asset, R. I. Chattot, J. Nelayah, N. Job, L. Dubau, F. Maillard, *ChemElectroChem* **2016**, *3*, 1591; b) L. Dubau, J. Nelayah, T. Asset, R. Chattot, F. Maillard, *ACS Catal.* **2017**, *7*, 3072; c) L. Dubau, T. Asset, R. Chattot, C. Bonnaud, V. Vanpeene, J. Nelayah, F. Maillard, *ACS Catal.* **2015**, *5*, 5333; d) R. Chattot, T. Asset, P. Bordet, J. Drnec, L. Dubau, F. Maillard, *ACS Catal.* **2017**, *7*, 398; e) T. Asset, R. Chattot, J. Drnec, P. Bordet, N. Job, F. Maillard, L. Dubau, *ACS Appl. Mater. Interfaces* **2017**, *9*, 25298.
- [14] A. Kongkanand, M. F. Mathias, *J. Phys. Chem. Lett.* **2016**, *7*, 1127.
- [15] B. Han, C. E. Carlton, A. Kongkanand, R. S. Kukreja, B. R. Theobald, L. Gan, R. O'Malley, P. Strasser, F. T. Wagner, Y. Shao-Horn, *Energy Environ. Sci.* **2015**, *8*, 258.
- [16] V. R. Stamenkovic, B. Fowler, B. S. Mun, G. F. Wang, P. N. Ross, C. A. Lucas, N. M. Markovic, *Science* **2007**, *315*, 493.
- [17] a) J. Zhang, H. Yang, J. Fang, S. Zou, *Nano Lett.* **2010**, *10*, 638; b) S.-I. Choi, S. Xie, M. Shao, J. H. Odell, N. Lu, H.-C. Peng, L. Protsailo, S. Guerrero, J. Park, X. Xia, J. Wang, M. J. Kim, Y. Xia, *Nano Lett.* **2013**, *13*, 3420; c) S.-I. Choi, S. Xie, M. Shao, N. Lu, S. Guerrero, J. H. Odell, J. Park, J. Wang, M. J. Kim, Y. Xia, *ChemSusChem* **2014**, *7*, 1476; d) C. Cui, L. Gan, M. Heggen, S. Rudi, P. Strasser, *Nat. Mater.* **2013**, *12*, 765.
- [18] L. Gan, C. Cui, M. Heggen, F. Dionigi, S. Rudi, P. Strasser, *Science* **2014**, *346*, 1502.
- [19] M. Asano, R. Kawamura, R. Sasakawa, N. Todoroki, T. Wadayama, *ACS Catal.* **2016**, *6*, 5285.
- [20] Q. Chang, Y. Xu, Z. Duan, F. Xiao, F. Fu, Y. Hong, J. Kim, S. I. Choi, D. Su, M. Shao, *Nano Lett.* **2017**, *17*, 3926.
- [21] L. Gan, C. H. Cui, M. Heggen, F. Dionigi, S. Rudi, P. Strasser, *Science* **2014**, *346*, 1502.
- [22] R. M. Arán-Ais, J. Solla-Gullón, M. Gocyla, M. Heggen, R. E. Dunin-Borkowski, P. Strasser, E. Herrero, J. M. Feliu, *Nano Energy* **2016**, *27*, 390.
- [23] L. Gan, M. Heggen, C. Cui, P. Strasser, *ACS Catal.* **2016**, *6*, 692.
- [24] M. Ahmadi, C. Cui, H. Mistry, P. Strasser, B. Roldan Cuenya, *ACS Nano* **2015**, *9*, 10686.
- [25] V. Beermann, M. Gocyla, S. Kuehl, E. Padgett, H. Schmies, M. Goerlin, N. Erini, M. Shviro, M. Heggen, R. E. Dunin-Borkowski, D. Muller, P. Strasser, *J. Am. Chem. Soc.* **2017**.
- [26] J. Park, J. Liu, H. C. Peng, L. Figueroa-Cosme, S. Miao, S. I. Choi, S. Bao, X. Yang, Y. Xia, *ChemSusChem* **2016**, *9*, 2209.
- [27] a) X. Huang, Z. Zhao, L. Cao, Y. Chen, E. Zhu, Z. Lin, M. Li, A. Yan, A. Zettl, Y. M. Wang, X. Duan, T. Mueller, Y. Huang, *Science* **2015**, *348*, 1230; b) Q. Jia, Z. Zhao, L. Cao, J. Li, S. Ghoshal, V. Davies, E. Stavitski, K. Attenkofer, Z. Liu, M. Li, X. Duan, S. Mukerjee, T. Mueller, Y. Huang, *Nano Lett.* **2018**, *18*, 798.
- [28] V. Beermann, M. Gocyla, E. Willinger, S. Rudi, M. Heggen, R. E. Dunin-Borkowski, M.-G. Willinger, P. Strasser, *Nano Lett.* **2016**, *16*, 1719.
- [29] J. Choi, Y. Lee, J. Kim, H. Lee, *J. Power Sources* **2016**, *307*, 883.
- [30] J. Lim, H. Shin, M. Kim, H. Lee, K. S. Lee, Y. Kwon, D. Song, S. Oh, H. Kim, E. Cho, *Nano Lett.* **2018**, *18*, 2450.
- [31] C. Zhang, W. Sandorf, Z. Peng, *ACS Catal.* **2015**, *5*, 2296.
- [32] M. Li, Z. Zhao, T. Cheng, A. Fortunelli, C.-Y. Chen, R. Yu, Q. Zhang, L. Gu, B. V. Merinov, Z. Lin, E. Zhu, T. Yu, Q. Jia, J. Guo, L. Zhang, W. A. Goddard, Y. Huang, X. Duan, *Science* **2016**, *354*, 1414.
- [33] a) N. Becknell, Y. Son, D. Kim, D. Li, Y. Yu, Z. Niu, T. Lei, B. T. Sneed, K. L. More, N. M. Markovic, V. R. Stamenkovic, P. Yang, *J. Am. Chem. Soc.* **2017**, *139*, 11678; b) N. Becknell, Y. Kang, C. Chen, J. Resasco, N. Kornienko, J. Guo, N. M. Markovic, G. A. Somorjai, V. R. Stamenkovic, P. Yang, *J. Am. Chem. Soc.* **2015**, *137*, 15817; c) Z. Niu, N. Becknell, Y. Yu, D. Kim, C. Chen, N. Kornienko, G. A. Somorjai, P. Yang, *Nat. Mater.* **2016**, *15*, 1188; d) X. Peng, S. Zhao, T. J. O'masta, J. M. Roller, W. E. Mustain, *Appl. Catal., B* **2017**, *203*, 927; e) H. Kwon, M. K. Kabiraz, J. Park, A. Oh, H. Baik, S. I. Choi, K. Lee, *Nano Lett.* **2018**, *18*, 2930; f) J. Park, M. Kanti Kabiraz, H. Kwon, S. Park, H. Baik, S. I. Choi, K. Lee, *ACS Nano* **2017**, *11*, 10844; g) F. Godinez-Salomon, R. Mendoza-Cruz, M. J. Arellano-Jimenez, M. Jose-Yacamán, C. P. Rhodes, *ACS Appl. Mater. Interfaces* **2017**, *9*, 18660; h) C. Wang, L. Zhang, H. Yang, J. Pan, J. Liu, C. Dotse, Y. Luan, R. Gao, C. Lin, J. Zhang, J. P. Kilcrease, X. Wen, S. Zou, J. Fang, *Nano Lett.* **2017**, *17*, 2204; i) A. Oh, H. Baik, D. S. Choi, J. Y. Cheon, B. Kim, H. Kim, S. J. Kwon, S. H. Joo, Y. Jung, K. Lee, *ACS Nano* **2015**, *9*, 2856; j) C. Chen, Y. J. Kang, Z. Y. Huo, Z. W. Zhu, W. Y. Huang, H. L. L. Xin, J. D. Snyder, D. G. Li, J. A. Herron, M. Mavrikakis, M. F. Chi, K. L. More, Y. D. Li, N. M. Markovic, G. A. Somorjai, P. D. Yang, V. R. Stamenkovic, *Science* **2014**, *343*, 1339.
- [34] a) C. Wang, G. F. Wang, D. van der Vliet, K. C. Chang, N. M. Markovic, V. R. Stamenkovic, *Phys. Chem. Chem. Phys.* **2010**, *12*, 6933; b) C. Wang, M. Chi, D. Li, D. van der Vliet, G. Wang, Q. Lin, J. F. Mitchell, K. L. More, N. M. Markovic, V. R. Stamenkovic, *ACS Catal.* **2011**, *1*, 1355; c) M. Chi, C. Wang, Y. Lei, G. Wang, D. Li, K. L. More, A. Lupini, L. F. Allard, N. M. Markovic, V. R. Stamenkovic, *Nat. Commun.* **2015**, *6*, 8925; d) S. Chen, P. J. Ferreira, W. Sheng, N. Yabuuchi, L. F. Allard, Y. Shao-Horn, *J. Am. Chem. Soc.* **2008**, *130*, 13818; e) R. Lin, T. Zhao, M. Shang, J. Wang, W. Tang, V. E. Guterma, J. Ma, *J. Power Sources* **2015**, *293*, 274; f) D. Yang, Z. Yan, B. Li, D. C. Higgins, J. Wang, H. Lv, Z. Chen, C. Zhang, *Int. J. Hydrogen Energy* **2016**, *41*, 18592; g) B. Li, Z. Yan, Q. Xiao, J. Dai, D. Yang, C. Zhang, M. Cai, J. Ma, *J. Power Sources* **2014**, *270*, 201; h) L. Dubau, F. Maillard, M. Chatenet, J. André, E. Rossinot, *Electrochim. Acta* **2010**, *56*, 776; i) J. W. Kim, J. H. Heo, S. J. Hwang, S. J. Yoo, J. H. Jang, J. S. Ha, S. Jang, T.-H. Lim, S. W. Nam, S.-K. Kim, *Int. J. Hydrogen Energy* **2011**, *36*, 12088; j) F. Maillard, L. Dubau, J. Durst, M. Chatenet, J. André, E. Rossinot, *Electrochem. Commun.* **2010**, *12*, 1161; k) S. Woo, I. Kim, J. K. Lee, S. Bong, J. Lee, H. Kim, *Electrochim. Acta* **2011**, *56*, 3036; l) M. Oezaslan, P. Strasser, *J. Power Sources* **2011**, *196*, 5240; m) I. Spanos, J. J. K. Kirkensgaard, K. Mortensen, M. Arenz, *J. Power Sources* **2014**, *245*, 908.
- [35] D. Wang, H. L. Xin, R. Hovden, H. Wang, Y. Yu, D. A. Muller, F. J. DiSalvo, H. D. Abruna, *Nat. Mater.* **2013**, *12*, 81.
- [36] N. Becknell, C. Zheng, C. Chen, Y. Yu, P. Yang, *Surf. Sci.* **2016**, *648*, 328.
- [37] M. Oezaslan, M. Heggen, P. Strasser, *J. Am. Chem. Soc.* **2012**, *134*, 514.
- [38] Y. Cai, P. Gao, F. Wang, H. Zhu, *Electrochim. Acta* **2017**, *245*, 924.
- [39] L. Wang, W. Gao, Z. Liu, Z. Zeng, Y. Liu, M. Giroux, M. Chi, G. Wang, J. Greeley, X. Pan, C. Wang, *ACS Catal.* **2018**, *8*, 35.
- [40] S. Rasouli, R. A. Ortiz Godoy, Z. Yang, M. Gummalla, S. C. Ball, D. Myers, P. J. Ferreira, *J. Power Sources* **2017**, *343*, 571.
- [41] X. X. Wang, S. Hwang, Y. T. Pan, K. Chen, Y. He, S. Karakalos, H. Zhang, J. S. Spendelov, D. Su, G. Wu, *Nano Lett.* **2018**, *18*, 4163.
- [42] Z. Li, R. Zeng, L. Wang, L. Jiang, S. Wang, X. Liu, *Int. J. Hydrogen Energy* **2016**, *41*, 21394.
- [43] M. Wakisaka, S. Kobayashi, S. Morishima, Y. Hyuga, D. A. Tryk, M. Watanabe, A. Iiyama, H. Uchida, *Electrochem. Commun.* **2016**, *67*, 47.
- [44] S. Kobayashi, M. Wakisaka, D. A. Tryk, A. Iiyama, H. Uchida, *J. Phys. Chem. C* **2017**, *121*, 11234.
- [45] Q. Chen, Z. Cao, G. Du, Q. Kuang, J. Huang, Z. Xie, L. Zheng, *Nano Energy* **2017**, *39*, 582.

- [46] Y. Qin, X. Zhang, X. Dai, H. Sun, Y. Yang, X. Li, Q. Shi, D. Gao, H. Wang, N. F. Yu, S. G. Sun, *Small* **2016**, 12, 524.
- [47] L. Bu, S. Guo, X. Zhang, X. Shen, D. Su, G. Lu, X. Zhu, J. Yao, J. Guo, X. Huang, *Nat. Commun.* **2016**, 7, 11850.
- [48] V. Yarlagadda, M. K. Carpenter, T. E. Moylan, R. S. Kukreja, R. Koestner, W. Gu, L. Thompson, A. Kongkanand, *ACS Energy Lett.* **2018**, 3, 618.
- [49] T. R. Garrick, T. E. Moylan, M. K. Carpenter, A. Kongkanand, *J. Electrochem. Soc.* **2017**, 164, F55.
- [50] K.-C. Wang, H.-C. Huang, C.-H. Wang, *Int. J. Hydrogen Energy* **2017**, 42, 11771.
- [51] X. Tan, S. Prabhudev, A. Kohandehghan, D. Karpuzov, G. A. Botton, D. Mitlin, *ACS Catal.* **2015**, 5, 1513.
- [52] R. M. Arán-Ais, F. Dionigi, T. Merzdorf, M. Gocyla, M. Heggen, R. E. Dunin-Borkowski, M. Gliach, J. Solla-Gullón, E. Herrero, J. M. Feliu, P. Strasser, *Nano Lett.* **2015**.
- [53] Z. Zhao, M. Feng, J. Zhou, Z. Liu, M. Li, Z. Fan, O. Tsen, J. Miao, X. Duan, Y. Huang, *Chem. Commun.* **2016**, 52, 11215.
- [54] K. Jiang, D. Zhao, S. Guo, X. Zhang, X. Zhu, J. Guo, G. Lu, X. Huang, *Sci. Adv.* **2017**, 3, e1601705.
- [55] M. Lokanathan, I. M. Patil, M. Navaneethan, V. Parey, R. Thapa, B. Kakade, *Nano Energy* **2018**, 43, 219.
- [56] a) M. Oezaslan, F. Hasche, P. Strasser, *J. Electrochem. Soc.* **2012**, 159, B444; b) M. Oezaslan, F. d. r. Hasché, P. Strasser, *Chem. Mater.* **2011**, 23, 2159; c) A. Sarkar, A. Manthiram, *J. Phys. Chem. B* **2010**, 114, 4725; d) G. Gupta, D. A. Slanac, P. Kumar, J. D. Wiggins-Camacho, X. Wang, S. Swinnea, K. L. More, S. Dai, K. J. Stevenson, K. P. Johnston, *Chem. Mater.* **2009**, 21, 4515; e) M. Oezaslan, M. Heggen, P. Strasser, *J. Am. Chem. Soc.* **2012**, 134, 514; f) H. El-Deeb, M. Bron, *J. Power Sources* **2015**, 275, 893; g) V. V. Pryadchenko, V. V. Sraibionyan, A. A. Kurzin, N. V. Bulat, D. B. Shemet, L. A. Avakyan, S. V. Belenov, V. A. Volochaev, I. Zizak, V. E. Guterman, L. A. Bugaev, *Appl. Catal. A: Gen.* **2016**, 525, 226; h) L. Liu, G. Samjeské, S. Takao, K. Nagasawa, Y. Iwasawa, *J. Power Sources* **2014**, 253, 1; i) Z. Xu, H. Zhang, S. Liu, B. Zhang, H. Zhong, D. S. Su, *Int. J. Hydrogen Energy* **2012**, 37, 17978; j) B. Chen, D. Cheng, J. Zhu, *J. Power Sources* **2014**, 267, 380.
- [57] A. H. A. Monte Verde Videla, R. Alipour Moghadam Esfahani, I. Peter, S. Specchia, *Electrochim. Acta* **2015**, 177, 51.
- [58] H. El-Deeb, M. Bron, *Electrochim. Acta* **2015**, 164, 315.
- [59] Y. Sohn, J. H. Park, P. Kim, J. B. Joo, *Curr. Appl. Phys.* **2015**, 15, 993.
- [60] J.-Y. Lee, S.-B. Han, D.-H. Kwak, M.-C. Kim, S. Lee, J.-Y. Park, I.-A. Choi, H.-S. Park, K.-W. Park, *J. Alloys Compd.* **2017**, 691, 26.
- [61] T. Lim, O.-H. Kim, Y.-E. Sung, H.-J. Kim, H.-N. Lee, Y.-H. Cho, O. J. Kwon, *J. Power Sources* **2016**, 316, 124.
- [62] Y. Zhou, D. Zhang, *J. Power Sources* **2015**, 278, 396.
- [63] Y. Li, F. Quan, K. Chen, L. Chen, C. Chen, *Catal. Today* **2016**, 278, 247.
- [64] Y. L. B. Kirchhoff, D. Fantauzzi, L. Calvillo, L. A. Estudillo-Wong, G. Granozzi, T. Jacob, N. Alonso-Vante, *ChemSusChem* **2018**, 11, 193.
- [65] Y. Li, F. Quan, E. Zhu, L. Chen, Y. Huang, C. Chen, *Nano Res.* **2015**, 8, 3342.
- [66] B.-A. Lu, T. Sheng, N. Tian, Z.-C. Zhang, C. Xiao, Z.-M. Cao, H.-B. Ma, Z.-Y. Zhou, S.-G. Sun, *Nano Energy* **2017**, 33, 65.
- [67] a) J. Kim, C. Rong, J. P. Liu, S. Sun, *Adv. Mater.* **2009**, 21, 906; b) S. Sun, C. B. Murray, D. Weller, L. Folks, A. Moser, *Science* **2000**, 287, 1989.
- [68] a) J. Kim, Y. Lee, S. Sun, *J. Am. Chem. Soc.* **2010**, 132, 4996; b) C. b. Rong, D. Li, V. Nandwana, N. Poudyal, Y. Ding, Z. L. Wang, H. Zeng, J. P. Liu, *Adv. Mater.* **2006**, 18, 2984.
- [69] a) S. Prabhudev, M. Bugnet, C. Bock, G. A. Botton, *ACS Nano* **2013**, 7, 6103; b) S. Zhang, X. Zhang, G. Jiang, H. Zhu, S. Guo, D. Su, G. Lu, S. Sun, *J. Am. Chem. Soc.* **2014**, 136, 7734.
- [70] J. Kim, C. Rong, Y. Lee, J. P. Liu, S. Sun, *Chem. Mater.* **2008**, 20, 7242.
- [71] a) Q. Li, L. Wu, G. Wu, D. Su, H. Lv, S. Zhang, W. Zhu, A. Casimir, H. Zhu, A. Mendoza-Garcia, S. Sun, *Nano Lett.* **2015**, 15, 2468; b) Y. Hu, J. O. Jensen, W. Zhang, L. N. Cleemann, C. Pan, Q. Li, *ChemCatChem* **2016**, 8, 3131.
- [72] H. Duan, Q. Hao, C. Xu, *J. Power Sources* **2014**, 269, 589.
- [73] D. Y. Chung, S. W. Jun, G. Yoon, S. G. Kwon, D. Y. Shin, P. Seo, J. M. Yoo, H. Shin, Y. H. Chung, H. Kim, B. S. Mun, K. S. Lee, N. S. Lee, S. J. Yoo, D. H. Lim, K. Kang, Y. E. Sung, T. Hyeon, *J. Am. Chem. Soc.* **2015**, 137, 15478.
- [74] Q. Wang, S. Chen, F. Shi, K. Chen, Y. Nie, Y. Wang, R. Wu, J. Li, Y. Zhang, W. Ding, Y. Li, L. Li, Z. Wei, *Adv. Mater.* **2016**, 28, 10673.
- [75] P. Malacrida, M. Escudero-Escribano, A. Verdaguer-Casadevall, I. E. L. Stephens, I. Chorkendorff, *J. Mater. Chem. A* **2014**, 2, 4234.
- [76] J. Greeley, I. E. L. Stephens, A. S. Bondarenko, T. P. Johansson, H. A. Hansen, T. F. Jaramillo, J. Rossmeisl, I. Chorkendorff, J. K. Nørskov, *Nat. Chem.* **2009**, 1, 552.
- [77] I. E. L. Stephens, A. S. Bondarenko, L. Bech, I. Chorkendorff, *ChemCatChem* **2012**, 4, 341.
- [78] M. Escudero-Escribano, P. Malacrida, M. H. Hansen, U. G. Vej-Hansen, A. Velazquez-Palenzuela, V. Tripkovic, J. Schiotz, J. Rossmeisl, I. E. L. Stephens, I. Chorkendorff, *Science* **2016**, 352, 73.
- [79] B. Garlyyev, M. D. Pohl, V. Colic, Y. C. Liang, F. K. Butt, A. Holleitner, A. S. Bandarenka, *Electrochem. Commun.* **2018**, 88, 10.
- [80] a) E. T. Ulrikkeholm, A. F. Pedersen, U. G. Vej-Hansen, M. Escudero-Escribano, I. E. L. Stephens, D. Friebel, A. Mehta, J. Schiotz, R. K. Feidenhansl, A. Nilsson, I. Chorkendorff, *Surf. Sci.* **2016**, 652, 114; b) T. P. Johansson, E. T. Ulrikkeholm, P. Hernandez-Fernandez, M. Escudero-Escribano, P. Malacrida, I. E. L. Stephens, I. Chorkendorff, *Phys. Chem. Chem. Phys.* **2014**, 16, 13718.
- [81] a) N. Lindahl, E. Zamburlini, L. G. Feng, H. Gronbeck, M. Escudero-Escribano, I. E. L. Stephens, I. Chorkendorff, C. Langhammer, B. Wickman, *Adv. Mater. Interfaces* **2017**, 4; b) E. Zamburlini, K. D. Jensen, I. E. L. Stephens, I. Chorkendorff, M. Escudero-Escribano, *Electrochim. Acta* **2017**, 247, 708; c) S. J. Yoo, S. K. Kim, T. Y. Jeon, S. J. Hwang, J. G. Lee, S. C. Lee, K. S. Lee, Y. H. Cho, Y. E. Sung, T. H. Lim, *Chem. Commun.* **2011**, 47, 11414; d) N. Lindahl, B. Eriksson, H. Gronbeck, R. W. Lindstrom, G. Lindbergh, C. Lagergren, B. Wickman, *ChemSusChem* **2018**, 11, 1438.
- [82] C. Roy, B. P. Knudsen, C. M. Pedersen, A. Velazquez-Palenzuela, L. H. Christensen, C. D. Damsgaard, I. E. L. Stephens, I. Chorkendorff, *ACS Catal.* **2018**, 8, 2071.
- [83] P. Hernandez-Fernandez, F. Masini, D. N. McCarthy, C. E. Strebler, D. Friebel, D. Deiana, P. Malacrida, A. Nierhoff, A. Bodin, A. M. Wise, J. H. Nielsen, T. W. Hansen, A. Nilsson, I. E. L. Stephens, I. Chorkendorff, *Nat. Chem.* **2014**, 6, 732.
- [84] A. Velazquez-Palenzuela, F. Masini, A. F. Pedersen, M. Escudero-Escribano, D. Deiana, P. Malacrida, T. W. Hansen, D. Friebel, A. Nilsson, I. E. L. Stephens, I. Chorkendorff, *J. Catal.* **2015**, 328, 297.
- [85] a) R. Cui, L. Mei, G. Han, J. Chen, G. Zhang, Y. Quan, N. Gu, L. Zhang, Y. Fang, B. Qian, X. Jiang, Z. Han, *Sci. Rep.* **2017**, 7, 41862; b) M. Tsuji, K. Uto, T. Nagami, A. Muto, H. Fukushima, J. Hayashi, *ChemCatChem* **2017**, 9, 962; c) R. Sandstrom, E. Gracia-Espino, G. Z. Hu, A. Shchukarev, J. Y. Ma, T. Wagberg, *Nano Energy* **2018**, 46, 141; d) R. Brandiele, C. Durante, E. Gradzka, G. A. Rizzi, J. Zheng, D. Badocco, P. Centomo, P. Pastore, G. Granozzi, A. Gennaro, *J. Mater. Chem. A* **2016**, 4, 12232; e) S. B. Han, D. H. Kwak, Y. W. Lee, S. J. Kim, J. Y. Lee, S. Lee, H. J. Kwon, K. W. Park, *Int. J. Electrochem. Sci.*

- 2016, 11, 3803; f) P. Ashok, P. Divya, S. Ramaprabhu, *J. Nanosci. Nanotechnol.* **2016**, 16, 9642.
- [86] J. S. Kanady, P. Leidinger, A. Haas, S. Titlbach, S. Schunk, K. Schierle-Arndt, E. J. Crumlin, C. H. Wu, A. P. Alivisatos, *J. Am. Chem. Soc.* **2017**, 139, 5672.
- [87] L. Asen, W. Ju, E. Mostafa, S. Martens, U. Heiz, U. Stimming, O. Schneider, *ECS Trans.* **2016**, 75, 323.
- [88] U. G. Vej-Hansen, M. Escudero-Escribano, A. Velazquez-Palenzuela, P. Malacrida, J. Rossmeisl, I. E. L. Stephens, I. Chorkendorff, J. Schiøtz, *Electrocatalysis* **2017**, 8, 594.
- [89] a) P. Strasser, S. Koh, T. Anniyev, J. Greeley, K. More, C. F. Yu, Z. C. Liu, S. Kaya, D. Nordlund, H. Ogasawara, M. F. Toney, A. Nilsson, *Nat. Chem.* **2010**, 2, 454; b) X. Zhang, G. Lu, *J. Phys. Chem. Lett.* **2014**, 5, 292.
- [90] L. Z. Bu, Q. Shao, E. Bin, J. Guo, J. L. Yao, X. Q. Huang, *J. Am. Chem. Soc.* **2017**, 139, 9576.
- [91] L. Z. Bu, N. Zhang, S. J. Guo, X. Zhang, J. Li, J. L. Yao, T. Wu, G. Lu, J. Y. Ma, D. Su, X. Q. Huang, *Science* **2016**, 354, 1410.
- [92] F. Ando, T. Tanabe, T. Gunji, S. Kaneko, T. Takeda, T. Ohsaka, F. Matsumoto, *ACS Appl. Nano Mater.* **2018**, 1, 2844.
- [93] S. X. Bao, M. Vara, X. Yang, S. Zhou, L. Figueroa-Cosme, J. Park, M. Luo, Z. X. Xie, Y. N. Xia, *ChemCatChem* **2017**, 9, 414.
- [94] K. Y. Cho, Y. S. Yeom, H. Y. Seo, P. Kumar, A. S. Lee, K. Y. Baek, H. G. Yoon, *ACS Appl. Mater. Interfaces* **2017**, 9, 1524.
- [95] S. F. Liu, W. P. Xiao, J. Wang, J. Zhu, Z. X. Wu, H. L. Xin, D. L. Wang, *Nano Energy* **2016**, 27, 475.
- [96] J. Park, M. Vara, Y. Xia, *Catal. Today* **2017**, 280, 266.
- [97] J. F. Wu, S. Y. Shan, H. Cronk, F. F. Chang, H. Kareem, Y. G. Zhao, J. Luo, V. Petkov, C. J. Zhong, *J. Phys. Chem. C* **2017**, 121, 14128.
- [98] M. Zhou, H. Wang, M. Vara, Z. D. Hood, M. Luo, T.-H. Yang, S. Bao, M. Chi, P. Xiao, Y. Zhang, Y. Xia, *J. Am. Chem. Soc.* **2016**, 138, 12263.
- [99] J. Park, L. Zhang, S. I. Choi, L. T. Røling, N. Lu, J. A. Herron, S. F. Xie, J. G. Wang, M. J. Kim, M. Mavrikakis, Y. N. Xia, *ACS Nano* **2015**, 9, 2635.
- [100] a) S. F. Xie, S. I. Choi, N. Lu, L. T. Røling, J. A. Herron, L. Zhang, J. Park, J. G. Wang, M. J. Kim, Z. X. Xie, M. Mavrikakis, Y. N. Xia, *Nano Lett.* **2014**, 14, 3570; b) X. Wang, S. I. Choi, L. T. Røling, M. Luo, C. Ma, L. Zhang, M. F. Chi, J. Y. Liu, Z. X. Xie, J. A. Herron, M. Mavrikakis, Y. N. Xia, *Nat. Commun.* **2015**, 6; c) H. Ataee-Esfahani, K. M. Koczkur, R. G. Weiner, S. E. Skrabalak, *ACS Omega* **2018**, 3, 3952.
- [101] a) J. Park, H. L. Wang, M. Vara, Y. N. Xia, *ChemSusChem* **2016**, 9, 2855; b) L. Zhang, L. T. Røling, X. Wang, M. Vara, M. F. Chi, J. Y. Liu, S. I. Choi, J. Park, J. A. Herron, Z. X. Xie, M. Mavrikakis, Y. N. Xia, *Science* **2015**, 349, 412.
- [102] a) Y. Hori, A. Murata, R. Takahashi, *J. Chem. Soc., Faraday Trans. 1*, **1989**, 85, 2309; b) Y. Hori, in *Modern Aspects of Electrochemistry*, Vol. 42 (Eds: C. Vayenas, R. White, M. Gamboa-Aldeco), Springer, New York **2008**, p. 89.
- [103] A. Bagger, W. Ju, A. S. Varela, P. Strasser, J. Rossmeisl, *ChemPhysChem* **2017**, 18, 3266.
- [104] a) R. Reske, H. Mistry, F. Behafarid, B. Roldan Cuenya, P. Strasser, *J. Am. Chem. Soc.* **2014**, 136, 6978; b) H. Mistry, A. S. Varela, C. S. Bonifacio, I. Zegkinoglou, I. Sinev, Y.-W. Choi, K. Kisslinger, E. A. Stach, J. C. Yang, P. Strasser, B. Roldan Cuenya, *Nat. Commun.* **2016**, 7, 12123; c) H. Mistry, F. Behafarid, R. Reske, A. S. Varela, P. Strasser, B. Roldan Cuenya, *ACS Catal.* **2016**, 6, 1075; d) A. S. Varela, W. Ju, T. Reier, P. Strasser, *ACS Catal.* **2016**, 6, 2136; e) D. Gao, I. Zegkinoglou, N. J. Divins, F. Scholten, I. Sinev, P. Grosse, B. Roldan Cuenya, *ACS Nano* **2017**, 11, 4825; f) X. Wang, A. S. Varela, A. Bergmann, S. Kühl, P. Strasser, *ChemSusChem* **2017**, 10, 4642.
- [105] a) Y. Chen, M. W. Kanan, *J. Am. Chem. Soc.* **2012**, 134, 1986; b) C. H. Lee, M. W. Kanan, *ACS Catal.* **2015**, 5, 465; c) C. Ding, A. Li, S.-M. Lu, H. Zhang, C. Li, *ACS Catal.* **2016**, 6, 6438.
- [106] a) H. Mistry, R. Reske, Z. Zeng, Z.-J. Zhao, J. Greeley, P. Strasser, B. R. Cuenya, *J. Am. Chem. Soc.* **2014**, 136, 16473; b) C. Kim, H. S. Jeon, T. Eom, M. S. Jee, H. Kim, C. M. Friend, B. K. Min, Y. J. Hwang, *J. Am. Chem. Soc.* **2015**, 137, 13844; c) C. Kim, T. Eom, M. S. Jee, H. Jung, H. Kim, B. K. Min, Y. J. Hwang, *ACS Catal.* **2017**, 7, 779.
- [107] a) J. M. Spurgeon, B. Kumar, *Energy Environ. Sci.* **2018**, 11, 1536; b) M. Jouny, W. Luc, F. Jiao, *Ind. Eng. Chem. Res.* **2018**, 57, 2165.
- [108] a) R. Kortlever, I. Peters, S. Koper, M. T. M. Koper, *ACS Catal.* **2015**, 5, 3916; b) W. Luc, C. Collins, S. Wang, H. Xin, K. He, Y. Kang, F. Jiao, *J. Am. Chem. Soc.* **2017**, 139, 1885; c) M. Bernal, A. Bagger, F. Scholten, I. Sinev, A. Bergmann, M. Ahmadi, J. Rossmeisl, B. R. Cuenya, *Nano Energy* **2018**, 53, 27.
- [109] S. Rasul, D. H. Anjum, A. Jedidi, Y. Minenkov, L. Cavallo, K. Takanebe, *Angew. Chem., Int. Ed.* **2015**, 54, 2146.
- [110] A. Jedidi, S. Rasul, D. Masih, L. Cavallo, K. Takanebe, *J. Mater. Chem. A* **2015**, 3, 19085.
- [111] G. O. Larrazábal, A. J. Martín, S. Mitchell, R. Hauert, J. Pérez-Ramírez, *ACS Catal.* **2016**, 6, 6265.
- [112] Z. B. Hoffman, T. S. Gray, K. B. Moraveck, T. B. Gunnoe, G. Zangari, *ACS Catal.* **2017**, 7, 5381.
- [113] S. Sarfraz, A. T. Garcia-Esparza, A. Jedidi, L. Cavallo, K. Takanebe, *ACS Catal.* **2016**, 6, 2842.
- [114] Q. Li, J. Fu, W. Zhu, Z. Chen, B. Shen, L. Wu, Z. Xi, T. Wang, G. Lu, J.-j. Zhu, S. Sun, *J. Am. Chem. Soc.* **2017**, 139, 4290.
- [115] J. Christophe, T. Doneux, C. Buess-Herman, *Electrocatalysis* **2012**, 3, 139.
- [116] F. Jia, X. Yu, L. Zhang, *J. Power Sources* **2014**, 252, 85.
- [117] G. Kyriacou, A. Anagnostopoulos, *J. Electroanal. Chem.* **1992**, 328, 233.
- [118] D. Friebel, F. Mbuga, S. Rajasekaran, D. J. Miller, H. Ogasawara, R. Alonso-Mori, D. Sokaras, D. Nordlund, T.-C. Weng, A. Nilsson, *J. Phys. Chem. C* **2014**, 118, 7954.
- [119] S. Lysgaard, J. S. Myrdal, H. A. Hansen, T. Vegge, *Phys. Chem. Chem. Phys.* **2015**, 17, 28270.
- [120] D. Kim, C. Xie, N. Becknell, Y. Yu, M. Karamad, K. Chan, E. J. Crumlin, J. K. Nørskov, P. Yang, *J. Am. Chem. Soc.* **2017**, 139, 8329.
- [121] H. Mistry, R. Reske, P. Strasser, B. Roldan Cuenya, *Catal. Today* **2017**, 288, 30.
- [122] J. Monzó, Y. Malewski, R. Kortlever, F. J. Vidal-Iglesias, J. Solla-Gullón, M. T. M. Koper, P. Rodriguez, *J. Mater. Chem. A* **2015**, 3, 23690.
- [123] D. Kim, J. Resasco, Y. Yu, A. M. Asiri, P. Yang, *Nat. Commun.* **2014**, 5, 4948.
- [124] Z. Chang, S. Huo, W. Zhang, J. Fang, H. Wang, *J. Phys. Chem. C* **2017**, 121, 11368.
- [125] E. L. Clark, C. Hahn, T. F. Jaramillo, A. T. Bell, *J. Am. Chem. Soc.* **2017**, 139, 15848.
- [126] D. Ren, B. S.-H. Ang, B. S. Yeo, *ACS Catal.* **2016**, 6, 8239.
- [127] T. T. H. Hoang, S. Verma, S. Ma, T. T. Fister, J. Timoshenko, A. I. Frenkel, P. J. A. Kenis, A. A. Gewirth, *J. Am. Chem. Soc.* **2018**, 140, 5791.
- [128] a) H. Hu, Y. Tang, Q. Hu, P. Wan, L. Dai, X. J. Yang, *Appl. Surf. Sci.* **2018**, 445, 281; b) G. Yin, H. Abe, R. Kodiyath, S. Ueda, N. Srinivasan, A. Yamaguchi, M. Miyauchi, *J. Mater. Chem. A* **2017**, 5, 12113; c) J. He, E. Dettelbach Kevin, A. Huang, P. Berlinguette Curtis, *Angew. Chem., Int. Ed.* **2017**, 56, 16579.
- [129] a) S. Pérez-Rodríguez, N. Rillo, M. J. Lázaro, E. Pastor, *Appl. Catal., B* **2015**, 163, 83; b) M. Rahaman, A. Dutta, P. Broekmann, *ChemSusChem* **2017**, 10, 1733; c) B. Jiang, X. G. Zhang, K. Jiang, D. Y. Wu, W. B. Cai, *J. Am. Chem. Soc.* **2018**, 140, 2880;

- d) C. Jiménez, J. García, R. Camarillo, F. Martínez, J. Rincón, *Energy Fuels* **2017**, *31*, 3038.
- [130] E. R. Cave, C. Shi, K. P. Kuhl, T. Hatsukade, D. N. Abram, C. Hahn, K. Chan, T. F. Jaramillo, *ACS Catal.* **2018**, *8*, 3035.
- [131] a) S. Taguchi, A. Aramata, M. Enyo, *J. Electroanal. Chem.* **1994**, *372*, 161; b) R. Kortlever, C. Balemans, Y. Kwon, M. T. M. Koper, *Catal. Today* **2015**, *244*, 58.
- [132] F. Cai, D. Gao, H. Zhou, G. Wang, T. He, H. Gong, S. Miao, F. Yang, J. Wang, X. Bao, *Chem. Sci.* **2017**, *8*, 2569.
- [133] a) F. Y. Zhang, T. Sheng, N. Tian, L. Liu, C. Xiao, B. A. Lu, B. B. Xu, Z. Y. Zhou, S. G. Sun, *Chem. Commun.* **2017**, *53*, 8085; b) X. Min, M. W. Kanan, *J. Am. Chem. Soc.* **2015**, *137*, 4701.
- [134] M. Li, J. Wang, P. Li, K. Chang, C. Li, T. Wang, B. Jiang, H. Zhang, H. Liu, Y. Yamauchi, N. Umezawa, J. Ye, *J. Mater. Chem. A* **2016**, *4*, 4776.
- [135] Z. Yin, D. Gao, S. Yao, B. Zhao, F. Cai, L. Lin, P. Tang, P. Zhai, G. Wang, D. Ma, X. Bao, *Nano Energy* **2016**, *27*, 35.
- [136] W. Zhu, L. Zhang, P. Yang, X. Chang, H. Dong, A. Li, C. Hu, Z. Huang, Z.-J. Zhao, J. Gong, *Small* **2018**, *14*, 1703314.
- [137] D. Chen, Q. Yao, P. Cui, H. Liu, J. Xie, J. Yang, *ACS Appl. Energy Mater.* **2018**, *1*, 883.
- [138] S. Ma, M. Sadakiyo, M. Heima, R. Luo, R. T. Haasch, J. I. Gold, M. Yamauchi, P. J. Kenis, *J. Am. Chem. Soc.* **2017**, *139*, 47.
- [139] Z. Weng, X. Zhang, Y. Wu, S. Huo, J. Jiang, W. Liu, G. He, Y. Liang, H. Wang, *Angew. Chem., Int. Ed.* **2017**, *56*, 13135.
- [140] H.-P. Yang, S. Qin, H. Wang, J.-X. Lu, *Green Chem.* **2015**, *17*, 5144.
- [141] X. Liu, L. Zhu, H. Wang, G. He, Z. Bian, *RSC Adv.* **2016**, *6*, 38380.
- [142] H.-P. Yang, S. Qin, Y.-N. Yue, L. Liu, H. Wang, J.-X. Lu, *Catal. Sci. Technol.* **2016**, *6*, 6490.
- [143] A. S. Varela, C. Schlaup, Z. P. Jovanov, P. Malacrida, S. Horch, I. E. L. Stephens, I. Chorkendorff, *J. Phys. Chem. C* **2013**, *117*, 20500.
- [144] X. Guo, Y. Zhang, C. Deng, X. Li, Y. Xue, Y.-M. Yan, K. Sun, *Chem. Commun.* **2015**, *51*, 1345.
- [145] R. Chattot, O. Le Bacq, V. Beermann, S. Kühl, J. Herranz, S. Henning, L. Kühn, T. Asset, L. Guétaz, G. Renou, J. Drnec, P. Bordet, A. Pasturel, A. Eychmüller, T. J. Schmidt, P. Strasser, L. Dubau, F. Maillard, *Nat. Mater.* **2018**, *17*, 827.
- [146] a) F. Calle-Vallejo, J. Tymoczko, V. Colic, Q. H. Vu, M. D. Pohl, K. Morgenstern, D. Loffreda, P. Sautet, W. Schuhmann, A. S. Bandarenka, *Science* **2015**, *350*, 185; b) F. Calle-Vallejo, M. D. Pohl, D. Reinisch, D. Loffreda, P. Sautet, A. S. Bandarenka, *Chem. Sci.* **2017**, *8*, 2283.
- [147] a) C. M. Zalitis, D. Kramer, A. R. Kucernak, *Phys. Chem. Chem. Phys.* **2013**, *15*, 4329; b) B. A. Pinaud, A. Bonakdarpour, L. Daniel, J. Sharman, D. P. Wilkinson, *J. Electrochem. Soc.* **2017**, *164*, F321; c) S. Martens, L. Asen, G. Ercolano, F. Dionigi, C. Zalitis, A. Hawkins, A. Martinez Bonastre, L. Seidl, A. C. Knoll, J. Sharman, P. Strasser, D. Jones, O. Schneider, *J. Power Sources* **2018**, *392*, 274.